Accepted Manuscript

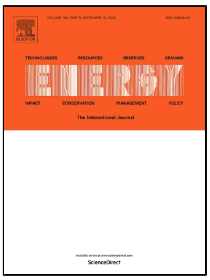

Thermo-mechanical behavior assessment of smart wire connected and busbar PV modules during production, transportation, and subsequent field loading stages

Guiqiang Li, M.W. Akram, Yi Jin, Xiao Chen, Changan Zhu, Ashfaq Ahmad, R.H. Arshad, Xudong Zhao

PII:	S0360-5442(18)32368-5
DOI:	10.1016/j.energy.2018.12.002
Reference:	EGY 14255
To appear in:	*Energy*
Received Date:	16 October 2018
Accepted Date:	01 December 2018

Please cite this article as: Guiqiang Li, M.W. Akram, Yi Jin, Xiao Chen, Changan Zhu, Ashfaq Ahmad, R.H. Arshad, Xudong Zhao, Thermo-mechanical behavior assessment of smart wire connected and busbar PV modules during production, transportation, and subsequent field loading stages, *Energy* (2018), doi: 10.1016/j.energy.2018.12.002

Thermo-mechanical behavior assessment of smart wire connected and busbar PV modules during production, transportation, and subsequent field loading stages

Guiqiang Li [†, b*], M. W. Akram[†, a, d], Yi Jin[a*], Xiao Chen[c], Changan Zhu[a], Ashfaq Ahmad[a], R. H. Arshad[d], Xudong Zhao[b]

[a]Department of Precision Machinery and Instrumentation, University of Science and Technology of China, 96 Jinzhai Road, Hefei, Anhui, 230026, China

[b]School of Engineering, University of Hull, Hull HU6 7RX, UK

[c]State Key Laboratory of Fire Science, University of Science and Technology of China, 96 Jinzhai Road, Hefei, Anhui, 230026, China

[d]Faculty of Agricultural Engineering, University of Agriculture Faisalabad, Jail Road, Faisalabad, 38000, Pakistan

*Corresponding authors

E-mail addresses: guiqiang.li@hull.ac.uk (G. Li), jinyi08@ustc.edu.cn (Y. Jin).

† Guiqiang Li and M. W. Akram contributed equally to this work, and they are co-first authors.

Abstract

Thermo-mechanical loads induce stresses in photovoltaic (PV) modules, leading to crack formation. In this context, the understanding of module's thermo-mechanical behavior is important. To investigate the thermo-mechanical behavior of smart wire connected technology (SWCT) and busbar PV modules throughout their entire life, the present study is conducted that probes the stress distribution and deformation during production, transportation, and subsequent mechanical and thermal loading stages in a consecutive step-by-step manner using finite element modelling approach. Pre-stresses and non-linearities are considered in simulation models. Stresses and displacements experienced by different parts/layers are examined, and crack sensitive regions are identified. In addition, the SWCT and busbar modules are compared, and it is found that SWCT interconnection is relatively a less stress inducing process and less susceptible to thermal and dynamic affects. During production stage, stresses of 39.3 MPa and 40.4 MPa are generated in SWCT cells and copper wires

respectively; while, stresses of 60 MPa and 87 MPa are generated in busbar cells and busbar respectively. Similarly, lower stresses are induced in SWCT PV modules during subsequent stages. The comparison results show advantages of SWCT module in terms of mechanical stability which can lead to improve the performance and reliability of PV modules.

Keywords: Thermo-mechanical behavior; Smart wire connected technology (SWCT) PV modules; Busbar PV modules; Production; Transportation; Mechanical and thermal loads.

1. Introduction

Conventional silicon solar cells are interconnected using three to five busbars through soldering technique. The soldering is a high temperature process which induces significant thermo-mechanical stresses in the cells leading to crack formation [1,2]. An effective alternative interconnection concept is smart wire connection technology (SWCT) [3,4] which involves interconnection through multiple copper wires during a low temperature lamination process. The SWCT cell manufacturing excludes the high temperature soldering process and replaces the busbars by a dense contact matrix of micro wires which makes it an attractive alternative in terms of less crack generation probability, enhanced current collection, and higher light trapping leading to higher power output and prolonged module life [5]. The SWCT cell typically consists of 15 to 38 copper wires [4] instead of busbars for conveying current. Therein, the solar cells are connected by means of foil-wire electrode to form a cell string and these strings are further interconnected during lamination.

The thermo-mechanical damage occurred during photovoltaic (PV) module manufacturing may not affect the output initially but with the passage of time the effect may become significant as PV module is subjected to environmental loads in the field [6]. This damage may cause power loss and effect the reliability of PV panels. As the photovoltaic (PV) industry tends towards use of reduced cell thickness from the last few years [7], the susceptibility to thermo-mechanical damage during subsequent handling, processing, and operation increases [8]. The mechanical stability of the PV modules can only be maintained, if the stresses generated due to thermo-mechanical loads in different materials remains

under their strength limits. The analysis of thermo-mechanical behavior in response to loads subjected during lifetime, and failure mechanisms can lead to address the related challenges.

The thermo-mechanical behavior of busbar PV module during manufacturing and subsequent life stages has been investigated in these studies: manufacturing process is analyzed by studies [9-16]; cracking effect on output or behavior is analyzed by studies [17-22]; behavior during application of different kind of loads is analyzed by studies [1,13,21-28]. However, the existing studies did not include the initial stresses or pre-stresses in their analysis except studies [9,11,16], but they [9,11,16] studied production stage only. The residual stress in a PV module is the result of the aggregation of residual stresses from each life stage [9] and the literature review shows lack of module behavior study covering its entire life. Therefore, a comprehensive study covering the thermo-mechanical aspects during the entire busbar PV module life in a consecutive step-by-step manner is required to gain a better understanding about module behavior.

On the other hand, the existing literatures are most concentrating on traditional busbar PV modules. A few studies [14,15,29,30] analyzed stresses induced in multi-busbar (multi-wire) PV modules during soldering. Cattaneo et al [31] and Papet et al [32] analyzed the feasibility of SWCT use with glass-glass lay-up and heterojunction cells respectively. Walter et al [33] analyzed mechanical stability of wire-based interconnection compared to ribbon interconnection in response to thermal loads. However, most of these studies are mainly focused on multi-busbar interconnection through soldering process or combination of SWCT with other design concepts. To the best of our knowledge gained through extensive literature review, there are no studies available about thermo-mechanical behavior of SWCT modules during manufacturing or subsequent stages. The information about behavior of SWCT PV modules is desirable due to their potential benefits [4,5] such as less stress generation probability, enhanced current collection, less silver consumption, and higher light trapping. Therefore, another detailed study is also required to analyze the thermo-mechanical behavior of SWCT cells during manufacturing, and subsequent life stages in a consecutive step-by-step manner.

In this context, the present study is carried out for in-depth investigation into thermo-mechanical behavior of SWCT, and busbar PV modules in response to loads subjected during manufacturing, handling, transportation, and subsequent mechanical and thermal loading stages in a consecutive step-by-step manner using finite element modelling approach. Different geometrical models are simulated for aforementioned stages in ANSYS [34]. Pre-stresses and non-linearities are considered in these simulation models. The thermo-mechanical stresses and displacements experienced by different layers of SWCT and busbar PV modules are probed. In addition, the simulated results for both kind of modules are compared, and crack sensitive regions are identified.

In summary, the objectives of present study are to: (1) assess thermo-mechanical behavior of SWCT and busbar PV modules during manufacturing, handling, transportation, and subsequent field loading in a consecutive step-by-step manner, (2) probe stresses and displacements experienced by different layers/parts of SWCT and busbar PV modules particularly, interconnecting copper wires and busbars in SWCT and busbar cells respectively, and (3) compare SWCT and busbar cells in terms of response to thermo-mechanical loads subjected during different life stages.

2. Theory of solid mechanics

The theory of solid mechanics gives relation between stresses, strains, and displacements of a solid body under the temperature changes, forces action, phase changes, and other internal/external phenomenon [35].

2.1 Governing equations

The governing equations of solid mechanics are balance of moment of momentum equation, kinematic compatibility equation, and constitutive equation [36]. They are given below.

Kinematic compatibility equation: The kinematic compatibility equation gives relation between strain and displacement as given in equation 1.

$$\varepsilon = \frac{1}{2}(\nabla\mu + (\nabla\mu)^{T}) \quad (1)$$

Where, Ɛ is strain tensor and μ is displacement vector.

Balance of moment of momentum equation: The balance of moment of momentum equation infers that the time derivative of moment of momentum is equal to sum of volumetric and external forces on a sub domain of a deformed solid body. Let Ω denote the subdomain of a deformed solid body, $\partial\Omega$ the surface of that subdomain, ρ the density, v the velocity (v = dμ/dt), ρb the internal forces acting on sub domain, and σ_n the external forces acting on surface of sub domain. Then, equation 2 will be produced.

$$\frac{d}{dt}\int_{\Omega}\rho v \, d\Omega = \int_{\Omega}\rho b \, d\Omega + \int_{\partial\Omega}\sigma_n dA \qquad (2)$$

With the Gaussian integral theorem and the definition of the stress tensor, $\sigma_n = n.\sigma$, equation 2 becomes as below:

$$\frac{d}{dt}\int_{\Omega}\rho v \, d\Omega = \int_{\Omega}(\rho b + \nabla.\sigma) \, d\Omega \qquad (3)$$

The balance is valid for any volumetric subset Ω of the body which is only possible if the integrand vanishes and then, equation 4 is obtained.

$$\rho\dot{v} = \nabla\cdot\sigma + \rho b \qquad (4)$$

Constitutive equation: The constitutive equation relates stresses with strains. For linear elastic materials, it is as below:

$$\sigma = C\varepsilon \qquad (5)$$

Where, C is the 4th order stiffness tensor. If the material is isotropic, C depends on only two parameters and equation (5) becomes as below:

$$\sigma = \lambda tr(\varepsilon)I + 2\mu\varepsilon \qquad (6)$$

The equation 6 represents Hooke's law. Therein, the operator tr(·) is the trace of a tensor. The two coefficients λ and μ are called Lamé constants.

The Hooke's law only deals with mechanical stress and strain, which infer that strain due to thermal loads does not produce any stress. However, the thermal load i.e. changes in temperature ($\Delta T = T - T_{ref}$) also results in thermal strain ($\varepsilon_{th} = \alpha \Delta TI$). By including thermal strain, equation 6 becomes as below:

$$\sigma = \lambda(\mathrm{tr}(\mathcal{E}) - 3\alpha\Delta T)I + 2\mu(\mathcal{E} - \alpha\Delta TI) \quad (7)$$

If a material is not a linear elastic material, different constitutive equations are used to model the behavior adequately.

2.2 Boundary and Initial conditions

The equation system (three sets of equations mentioned above i.e. 1, 4 and 7) of solid mechanics problem further consist of fifteen scalar equations. These are six compatibility equations, three balance of moment of momentum equations, and six constitutive equations. Therein, 15 unknowns are μ (3 components), σ (6 components), and $\mathcal{E}$ (6 components). For static solid mechanics problem, the left-hand side in balance of moment of momentum equation vanishes i.e. $\rho\dot{v} = 0$ [36].

Additionally, other conditions are required to get a unique mathematical problem. For static solid mechanics problems, boundary conditions are required; and for time-dependent solid mechanics problems, both initial and boundary conditions are required [36].

$$\mu|\,\Gamma_1 = g(x,t),\ x \in \Gamma_1 \quad (8)$$

$$\sigma.\,\mathrm{n}|\Gamma_2 = f(x,t),\ x \in \Gamma_2 \quad (9)$$

$$\mu(x,t_0) = h_1(x) \quad (10)$$

$$\dot{u}(x,t_0) = h_2(x) \quad (11)$$

The boundary Γ_1 represents the part of body where displacements are given and Γ_2 represents the part where stresses are applied.

3. Finite element models

Generally, problems of solid mechanics form a set of partial differential equations as given in section 2. These equations cannot be solved analytically except for simple geometry cases. Finite element method (FEM) is commonly used to solve such system of equations. The present study uses different FE models to simulate different processes and conditions in order to get best results. The pre-stresses are considered for these models according to the specific case. The manufacturing of SWCT cells includes only lamination process while that of busbar cells includes both soldering and lamination process. As, the soldering process is carried out on individual busbar cells, it is simulated on a simplified quarter busbar solar cell model using symmetry conditions. On the other hand, lamination process is carried out on the entire PV module in case of both busbar and SWCT cells, thus, it is simulated on a simplified quarter PV panel model using symmetry conditions. However, the simulation of transport and dynamic field conditions requires modal analysis in first step. The models simplified with symmetry conditions cannot give best results for modal analysis as mode shapes for a structure are not always symmetric. Thus, a full-scale PV panel model is used to simulate transport and dynamic field conditions. Moreover, the static and thermal field loads are also simulated on full-scale PV panel model.

The full-scale and quarter models of SWCT PV module have much less size in thickness direction as compared to planar directions; therefore, 4-node shell elements are used for all of their parts (cell, encapsulant, glass, and backsheet) except Cu wires. For their cu wires, beam elements are used. In full-scale and quarter models of busbar PV module, 4-node shell elements are used for all of their parts (cell, encapsulant, glass, and backsheet) except busbar and solder. For their busbars and solders, 8-node solid elements are used. In case of quarter model of busbar PV cell, 8-node solid elements are used. Furthermore, mesh refinement study is conducted in detail to achieve better results and avoid convergence issues.

The dimensions of model layers and parts for SWCT and busbar PV modules are given in table 1 and 2 respectively. Further details of geometrical models are given in section 4.

Table 1. Dimensions of model layers and parts for SWCT PV module

Model	Solar cell (L*W*T) mm	Encapsulant (L*W*T) mm	Cu wires (diameter) mm	Glass (L*W*T) mm	Backsheet (L*W*T) mm
Quarter SWCT PV module	156*156*0.18 (15 in No.)	809*493*1.38	0.2 mm (18 on each cell side i.e. front & back)	809*493*3.2	809*493*0.325
Full-scale SWCT module	156*156*0.2 (60 in No.)	1620*988*1.38	0.2 mm (18 on each cell side i.e. front & back)	1620*988*3.2	1620*988*0.325

Table 2. Dimensions of model layers and parts for Busbar (BB) PV module

Model	Solar cell (L*W*T) mm	Encapsulant (L*W*T) mm	Glass (L*W*T) mm	Backsheet (L*W*T) mm	Busbar (L*W*T) mm	Solder (L*W*T) Mm
Quarter Busbar PV cell	78*78*0.2	_	_	_	78*1.5*0.2 (1st) 78*0.75*0.2 (2nd)	78*1.5*0.014 (1st) 78*0.75*0.014 (2nd)
Quarter Busbar PV module	156*156*0.2 (15 in No.)	809*493 *1.428	809*493 *3.2	809*493 *0.325	156*1.5*0.2 (3 on each cell)	156*1.5*0.014 (3 on each cell)
Full-scale Busbar module	156*156*0.2 (60 in No.)	1620*988 *1.428	1620*988 *3.2	1620*988 *0.325	156*1.5*0.2 (3 on each cell)	156*1.5*0.014 (3 on each cell)

3.1 FEM Problems

The problems studied in our paper are of both static and dynamic structural categories. A static analysis calculates the impact of steady loads on a body. It ignores inertia and damping effects, such as those caused by time-varying loads. However, it includes those time-varying loads that can be approximated as static loads, for example static equivalent wind loads. Such analysis can be either linear or non-linear. Non-linearities like large deformation, plasticity, varying contact status, etc. can be considered.

On the other hand, structural dynamic problems consider time-varying loads. The equation of motion for a structural dynamic system, that is used in ANSYS, is given below [34].

$$[M].\ddot{u} + [C].\dot{u} + [K].u = f(t) \qquad (12)$$

Where, [M], [C], and [K] represents matrices of structural mass, structural damping, and structural stiffness respectively; and $\ddot{u}$, $\dot{u}$, and u represents vectors of nodal acceleration, nodal velocity, and nodal displacement respectively. $f(t)$ represents the applied load vector. Therein, [M], [C], and [K] are showing properties of the system, $\ddot{u}$, $\dot{u}$, and u shows system behavior, and $f(t)$ is the action. Different problems associated with structural dynamics can be formulated on the basis of equation 12. In our study, modal analysis, response spectrum analysis, and harmonic response analysis systems are used for solving dynamic problems.

A modal analysis determines the vibration behavior of a body i.e. natural frequencies and mode shapes. It acts as a basis for other detailed dynamic investigations. Therein, right-hand side of equation 12 is taken as zero i.e. $f(t) = 0$. Harmonic response analysis investigates the response of body experiencing steady-state vibrational loads. Therein, the expression used for applied load (right-hand side) is $f(t) = f_{max}.e^{i(\Omega t + \Psi)}$; where, f_{max} denotes force amplitude, Ω represents circular frequency (radians/time), and Ψ represents the force phase shift (radians). A spectrum analysis investigates dynamic behavior of a body experiencing random or time-dependent loads like dynamic wind forces. Therein, spectral quantities like acceleration vs frequency (capturing intensity and frequency content of time-history loads) are used in conjunction with modal analysis results.

3.2 Non-Linearity in the models

The common types of nonlinearities inherent in the mechanical systems are geometric nonlinearity, contact nonlinearity, and material nonlinearity. Depending upon the nature of problem analysis, geometric nonlinearity, and/or contact nonlinearity is considered in present study. The nonlinear strain-displacement relations give rise to geometric nonlinearity. Therein, displacement has nonlinear relationship with the applied load, resulting in large deflection. While, contact nonlinearity is associated with varying contact status leading to convergence failure.

The convergence issues experienced in our study, and steps followed to resolve them are given in table 3. These steps are tried in individual or in combination to achieve convergence.

Table 3. Convergence issues and solutions adopted in present study

Sr. No.	Convergence issue	Solution
1	Varying contact status	1. Modify normal stiffness factor 2. Refine mesh to achieve convergence
2	Degree of freedom (DOF) exceeded	1. Use bonded contact 2. Apply DOF constraints randomly 3. Add weak springs
3	Contact penetration	1. Reduce normal stiffness factor
4	Element shape error or large plastic strain	1. Apply load in smaller steps
5	Distortion of elements	1. Apply load in small steps 2. Modify mesh

3.3 Material properties

The materials used in different layers of studied models are glass, ethylene-vinyl acetate (EVA), copper, silicon, and solder (Sn95.5Ag3.8Cu0.7). The physical and mechanical properties of these materials are taken from literature as given in table 4. Glass is considered as an isotropic linear elastic material as it behaves as an elastic material below 550 ^{o}C and the temperature in every studied process remains below this limit. Silicon is considered as an elastic anisotropic material. Linear thermal expansion coefficients of silicon between 4 K to 340 K, 340 K to 850 K, 850 K to 1500 K are taken from literatures [37,38, and 39] respectively. Song et al [9] recommended to consider the copper as elastoplastic material. According to Tippabhotla et al [11], consideration of copper as just linear elastic material causes over prediction of results, as stiffness changes of inter-connector could not be accommodated upon yielding. Therefore, copper is considered as elastic perfectly plastic material. Temperature dependent coefficient of thermal expansion, and young's modulus is considered for

solder (Sn95.5Ag3.8Cu0.7) [40,41]. EVA, and backsheet are considered as temperature dependent elastic materials.

Table 4. Material properties

Material	Young's modulus (Gpa)	CTE (10^{-6} K^{-1})	Poisson ratio	Density (Kgm^{-3})
Silicon	Stiffness matrix (Anisotropy) [42]	Temp. dependent [37-39]	0.28 [13,23]	2330 [23]
Copper	117 [43,44]	17 [14,45]	0.35 [12]	8960 [46]
Solder (Sn95.5Ag3.8Cu0.7)	Temp. dependent [41]	Temp. dependent [40]	0.25	7370
Back sheet	3.5 [42]	50.4 [42]	0.29 [42]	2520 [42]
EVA	0.0677 [13,23]	270 [42]	0.33 [13,23]	922 [23]
Glass	73 [42]	8 [12,42]	0.23 [13,42]	2500 [12,42]

3. Simulation Methodology

This section discusses the simulation methodology for production, transportation, mechanical loading, and thermal loading of SWCT and busbar PV modules. Moreover, the geometrical models used in these stages are also discussed.

4.1 Module production

As mentioned earlier in section 3, the production process of busbar cells comprises both soldering and lamination while, that of SWCT cells includes lamination only. The soldering process for busbar cell is simulated on a simplified quarter cell model as shown in figure 1a. The symmetry conditions are applied in directions as shown in figure 1a. The model consists of solar cell (Silicon), busbars (Copper), and solders (Sn 95.5Ag3.8Cu0.7). Boundary conditions are applied to simulate real soldering process and avoid rigid body displacement i.e. condition of zero displacement is applied in one direction. Soldering is simulated in two steps; soldering step causing increase in temperature, and subsequent cooling step causing decrease in temperature due to convection. Therein, temperature is first increased from 25 ^{o}C to 220 ^{o}C in steps of 10 ^{o}C with consideration of soldering speed of 1.2 mm/sec to simulate

the thermal load caused by soldering step [10]. Subsequently, the model is cooled down to room temperature (25 °C) to simulate the heat transfer to room environment.

The lamination process for both busbar and SWCT cells are simulated on a simplified quarter PV panel model using symmetry conditions. The model used for simulating lamination process in busbar module is shown in figure 1b. The symmetry conditions are applied in directions as shown in figure 1b. The model consists of solar cell (Silicon), busbars (Copper), solders (Sn 95.5Ag3.8Cu0.7), encapsulant (EVA), glass, and back sheet. The solar cells, and busbars are embedded in encapsulant. Stresses induced during soldering process are considered. The lamination process is simulated in two steps; curing step i.e. heating up to lamination temperature (melting point of encapsulant), and subsequent cooling step i.e. cooling to room temperature. Therein, the temperature is first increased from 25 °C to 150 °C in steps of 10 °C to simulate melting of encapsulant. Afterwards, the cooling step is simulated.

The model used for simulating lamination process in SWCT PV module is shown in figure 1c. The symmetry conditions are applied in directions as shown in figure 1c. It consists of back sheet, encapsulant, Solar cells, Copper wires, and Glass. 18 copper wires are modelled on each side of the solar cell. The solar cells and copper wires are embedded in encapsulant. The lamination process is carried out in the same manner as for busbar module. Therein, the temperature is first increased to simulate the melting of encapsulant. Secondly, the temperature is decreased to room temperature to simulate convection between PV panel and room environment. The copper wires are connected to solar cells during this process.

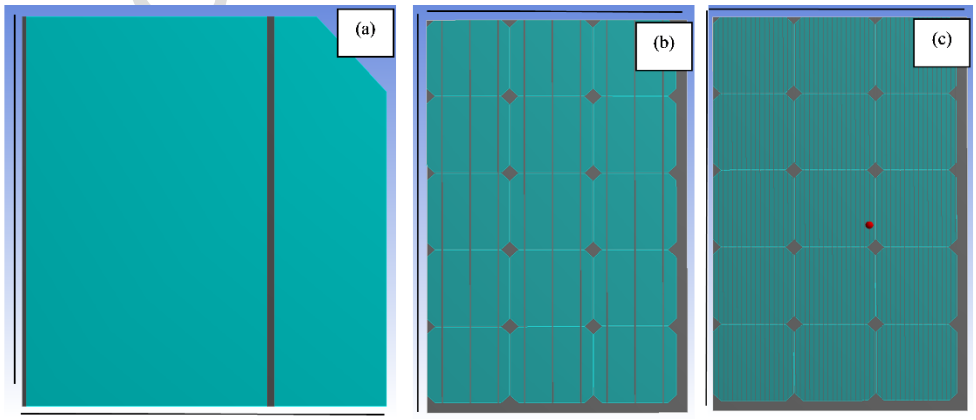

Figure 1. Geometrical models for busbar & SWCT cell/module (a) Quarter busbar PV cell (b) quarter busbar PV module (c) Quarter SWCT PV module. [Black lines near edges indicate symmetry conditions]

4.2 Transport

Transport is a critical stage in a PV module's life [17]. The glass of a PV panel or the solar cells may break due to vibrations and shocks during transportation [47]. Kontges et al [17] studied that the loads subjected during transport induce stresses which are the main cause of crack growth in solar panels. To simulate these loads, the impact of transportation is analyzed, as suggested by Kontges et al [48]. The shocks during handling and transport of PV modules are simulated to assess their effects. Full-scale PV panel models are used for both SWCT and busbar PV modules as shown in figure 2 and 3 respectively. Stresses induced during production stage of respective module type are considered accordingly. Boundary conditions are applied at the edges of both models to avoid displacement at edges as in real PV module due to presence of frame. Firstly, modal analysis is carried out for both models to extract mode shapes and calculate natural frequencies. Subsequently, the maximum amplitude of shocks is varied in steps of 5 m/s^2, 10 m/s^2, 20 m/s^2, and 30 m/s^2 in response spectrum analysis system to simulate shocks subjected during transportation. Therein, the shock length is varied between 2 ms and 36.5 ms in steps of 1.5 ms, and further, shock length of 40 ms and 45 ms is also taken. During response spectrum analysis, the corners of PV modules are rigidly fixed to simulate the condition of real shipping stack.

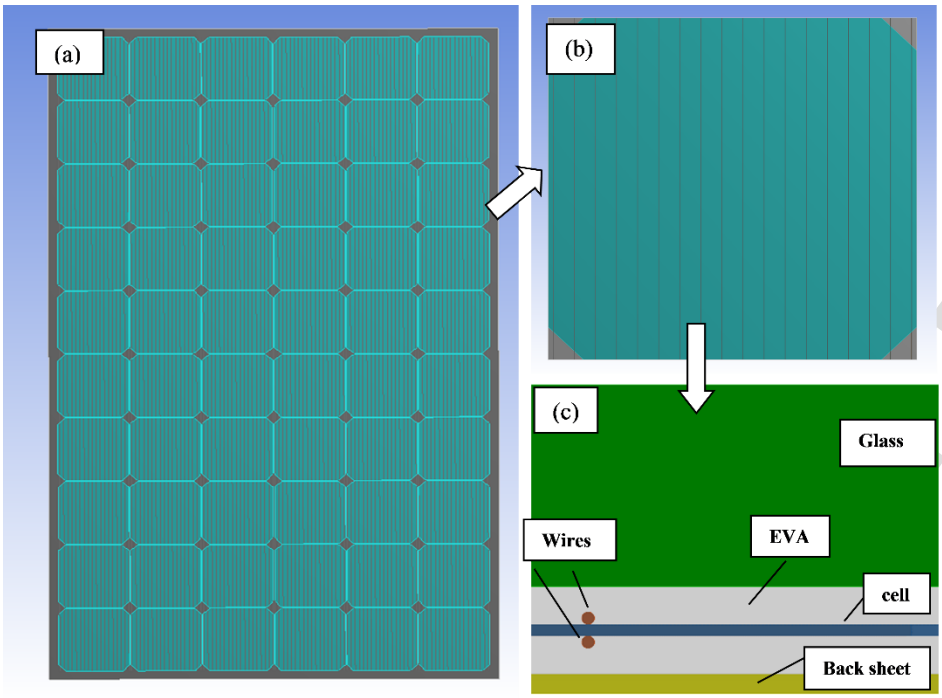

Figure 2. Full-scale geometrical model for SWCT PV module/cell (a) SWCT PV module (b) SWCT PV cell (c) Layers/parts of SWCT PV models.

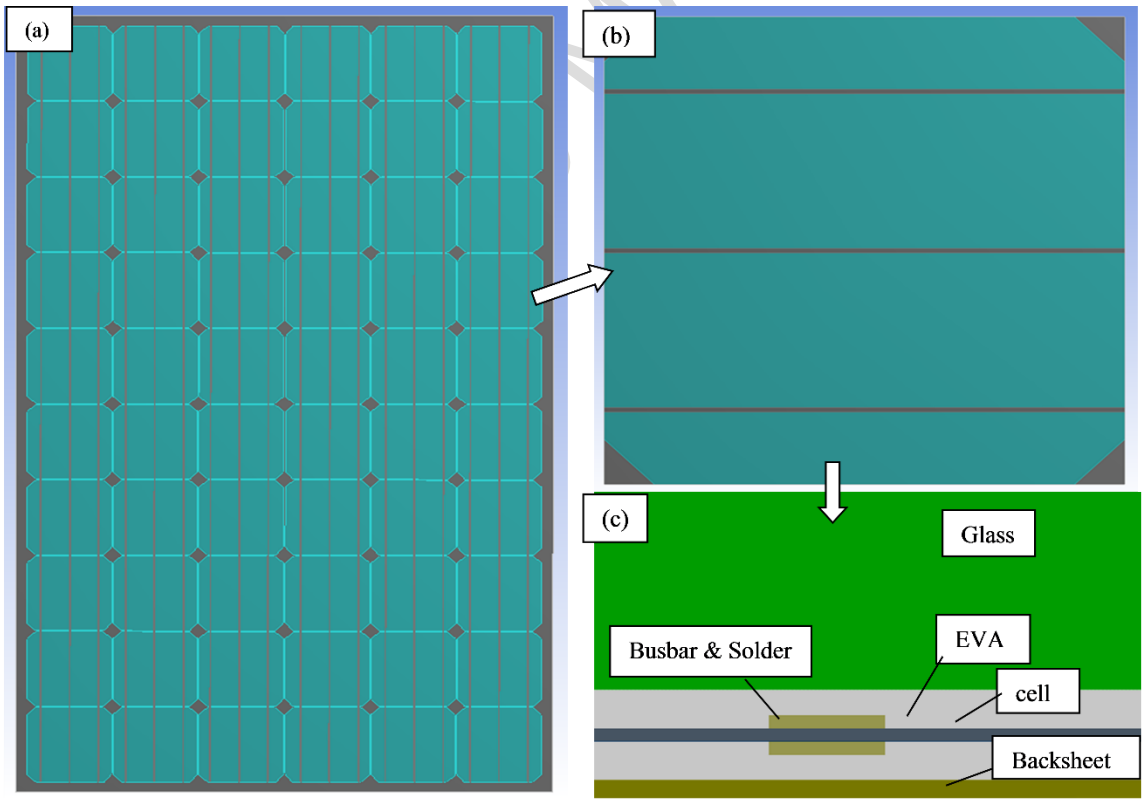

Figure 3. Full-scale geometrical model for busbar PV module/cell (a) Busbar PV module (b) Three busbar PV cell (c) Layers/parts of busbar PV models.

4.3 Static Loading

PV modules are subjected to wind and snow loads in the field after installation [49]. A mechanical load test is used to investigate the ability of PV module to withstand such loads in the field. The IEC 61215 standard mechanical load test [50] is simulated for analyzing the effect of these loads. To simulate these loads, full-scale solar panel models are used for both SWCT and busbar modules as shown in figure 2 and 3 respectively. Stresses induced during production stage are considered. According to IEC 61215 test [50], three pressure cycles are applied. During one cycle, a pressure of 2400 pa is applied for one hour on both front and rear faces of panel in two consecutive steps. For simulation of snow and ice loads, a pressure of 5400 pa is applied on the front face during last cycle. The load is applied in a gradual, uniform manner as required by standard test.

4.4 Dynamic Loading

The PV panels are subjected to static as well as dynamic loads in the field [51], but the IEC 61215 test [50] only covers static load conditions [25,47]. The studies [52,53] recommended to consider static as well as dynamic characteristics of PV modules. Therefore, dynamic loads are also considered in present study to simulate their effects. To simulate these loads, full-scale solar panel models are used for both SWCT and busbar modules as shown in figure 2 and 3 respectively. Stresses induced during production stage are considered. The impact of dynamic loads is analyzed as suggested by Dong et al [53]. According to study [53], a harmonic excitation with amplitude of 2400 pa and frequency sweep from 0 to 100 Hz is employed to simulate dynamic loads. The harmonic response analysis system is used for this purpose. The modes and natural frequencies extracted using modal analysis, as mentioned in section 4.2, are used in this harmonic analysis. This harmonic analysis gives knowledge about structural deformation and induced stresses for the entire frequency range of 0 to 100 Hz.

4.5 Thermal Loading

PV panel is subjected to extreme temperatures in the field, resulting in stress generation. Thermal cycling [50] is an environmental test to investigate thermal stresses generated in PV module due to

variation in extreme temperatures. It is a critical test for investigating interconnection technology. To simulate thermal loads, full-scale solar panel models are used for both SWCT and busbar modules as shown in figure 2 and 3 respectively. The models are subjected to IEC 61215 temperature cycling test [50] to simulate thermal loading. The cycling temperature limits are -40 ^{o}C and +85 ^{o}C. During a thermal cycle, the simulation temperature is decreased from +25 ^{o}C to -40 ^{o}C. Subsequently, the temperature is increased from -40 ^{o}C to +85 ^{o}C, and finally, the model is cooled down to +25 ^{o}C. The heating/cooling rate throughout the cycle is 100 ^{o}C/hour and the dwell time at both lower and upper temperature extremes is 10 minutes.

5 Results and discussion

In this section, thermo-mechanical behavior of different layers of SWCT and Busbar PV modules during production, transport, mechanical loading, and thermal loading are discussed.

5.1 Module Production

As mentioned in section 4.1, the SWCT PV module production is carried out during lamination process. During curing step, the EVA melts and flow around the cells, and interconnecting copper wires to fill the gaps. After lamination, the module is allowed to cool down to room temperature. This process induces high stresses in different layers of PV module. In solar cell matrix, the solar cells in the middle columns (3rd and 4th) experience high stresses as compared to other cells of the module. The cells in the middle columns experience maximum stresses of 39.32 MPa [See figure 4a]. During lamination, the EVA melts and flow around the cells to fill the gaps leading to interconnections under the action of lamination pressure. The encapsulant layer experiences maximum stresses of 2.1 MPa in the regions, where the cell gaps are located [See figure 4b]. The encapsulant layer undergoes displacement of 1.06 mm in center and outward region. A maximum deflection of 0.212 mm is found in glass region near the frame.

On the other hand, the copper wires over/under the cells located adjacent to frame and in the middle columns experience high stresses comparatively. Within each single cell, the copper wires at the outward side experience higher stresses near their ends. The maximum stress found in the copper wiring is 40.45 MPa [See figure 4c]. Furthermore, the copper wires present in the middle columns (3rd and 4th), and the outward columns located near the frame (1st and 6th) undergo higher deflection as compared to the wires in 2nd and 5th column. The maximum deflection found in the copper wires is 0.37 mm near their edges [see figure 4d]. Within each single cell, the copper wires at the outward side experience higher deflection near their ends. It can be clearly observed in figure 4d, which shows that this region is more sensitive to interconnection damage in SWCT cells.

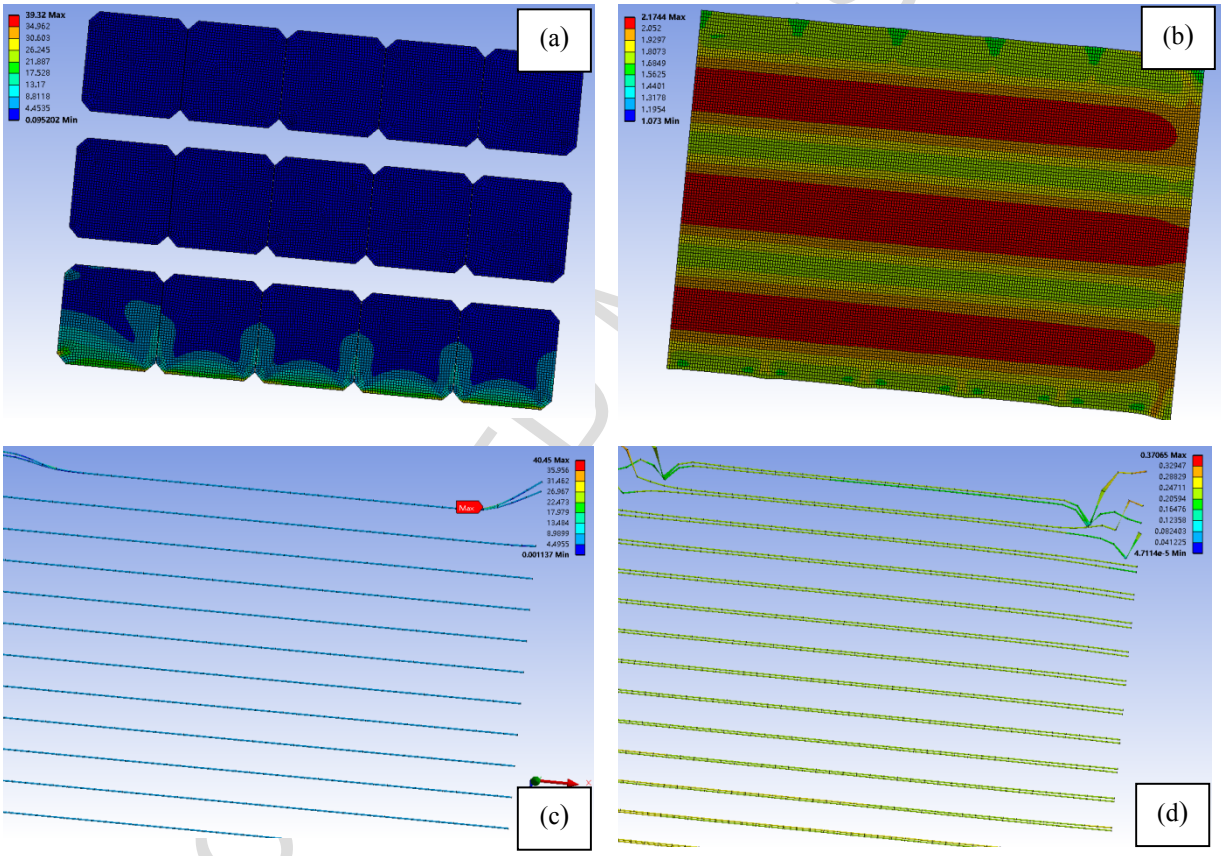

Figure 4. Stresses (MPa) and deformation (mm) in SWCT PV module during lamination (a) stress in solar cells (b) stress in encapsulant (c) stress in Cu wires (d) Deformation in Cu wires. [Upper right-hand quarter of complete module is shown in 4(a & b), and Cu wires of upper right-hand cell are shown in 4(c & d)]

In case of busbar PV module production, during soldering process, the solder passes over the solar cell. As it is a high temperature process, thermal stresses are generated in the solar cells and busbars when cooling step is carried out. Therein, stress development is due to mismatch of coefficient of

thermal expansion (CTE). Among three busbars, higher stresses are generated in the middle busbar. In busbars, the highest stress of magnitude 68.3 MPa is generated near the end of busbar [see figure 5a]. Moreover, the busbars undergo maximum displacement of 0.099 mm. In the solar cell, the highest stress of magnitude 44.9 MPa is generated in the cell region near the end of busbar [see figure 5b]. Moreover, the cell undergoes maximum displacement of 0.067 mm. The results show that the regions near busbar ends are crack sensitive points.

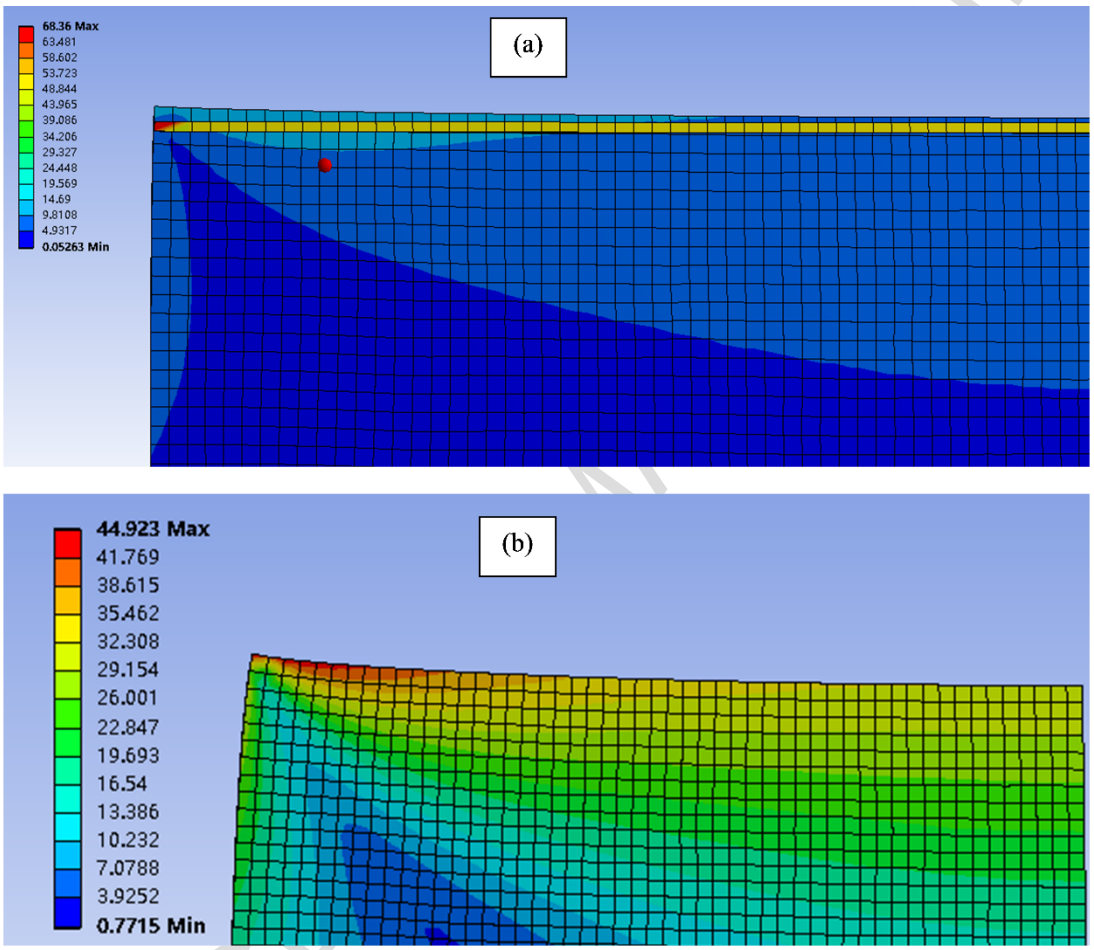

Figure 5. Stresses (MPa) generated in busbar solar cell during soldering process (a) stresses in busbar, (b) stresses in solar cell.

Subsequent to soldering, lamination process is carried out during production stage of busbar PV module. Therein, the EVA melts and flow around the cells and interconnectors to fill the gaps. During lamination process, thermo-mechanical stresses are induced in different layers of busbar module. In solar cell matrix, the cells located near the frame experience highest stresses and displacements. The

cells in the middle columns of the module experience approximately zero stress. The maximum stress of magnitude 59.7 MPa is found in solar cells near the frame [see figure 6a]. In case of busbars, higher stresses are found near the busbar end. The maximum stresses of magnitude 64.5 MPa and 87.2 MPa are found in the upper [see figure 6b] and lower [see figure 6d] busbars of the cells located near frame respectively. Furthermore, it was found that the lower busbars experience higher stresses and displacements as compared to the upper busbars in each cell. The displacement experienced by solar cells during lamination process is shown in figure 6c.

Apart from these layers, glass also experiences maximum stresses of 34.1 MPa near the frame. The middle region of glass layer experience compressive stress of 0.2 MPa. Due to this compressive stress, the middle region in the glass layer undergoes deformation of 0.4 mm. While, there is no deformation in the glass region near the module frame.

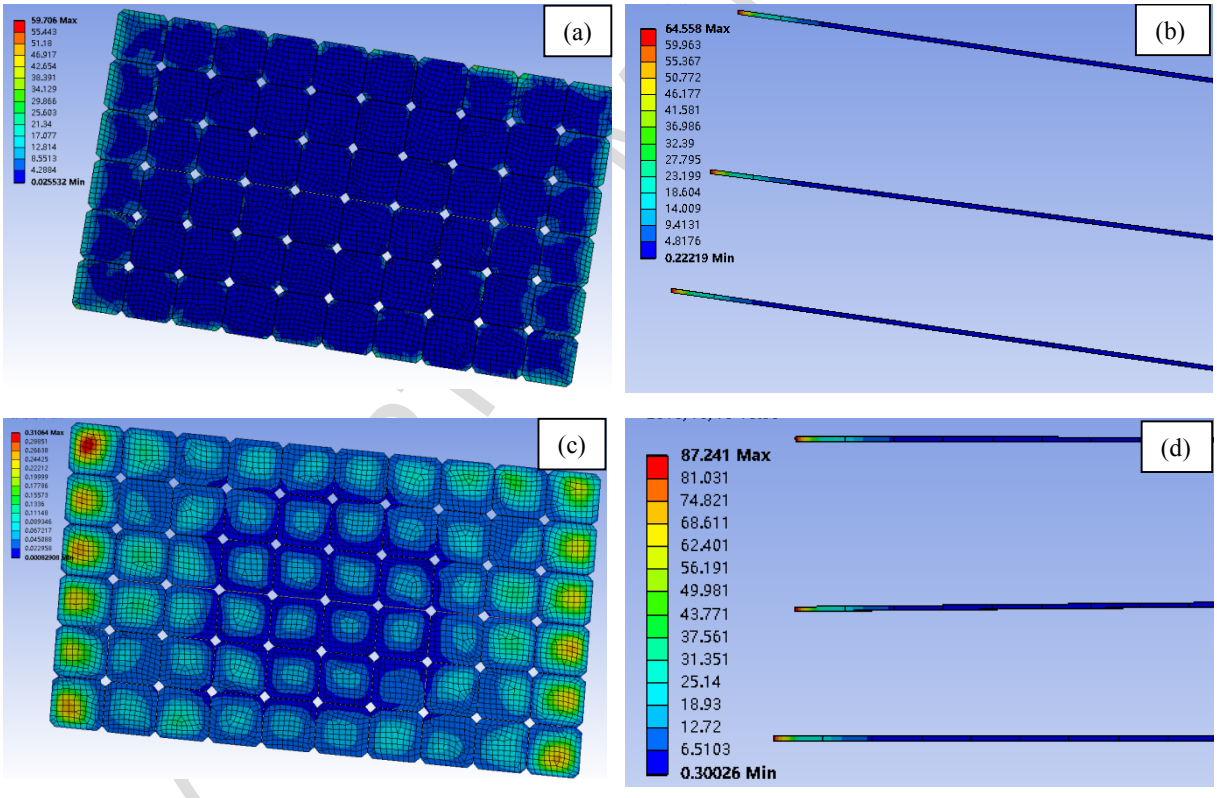

Figure 6. Stresses (MPa) and displacement (mm) in busbar module during lamination (a) stresses in solar cell (b) stresses in upper busbars (c) displacement in solar cells (d) stresses in lower busbars.

[busbar ends of cells located near frame are shown in 6(b & d)]

5.2 Transport

During transport and transport handling, the movement of PV modules causes cell and/or glass cracking. In present study, the SWCT and busbar PV modules are simulated for shocks during transportation and handling to analyze their effects. Firstly, modal analysis is carried out for both kind of panels to extract mode shapes and calculate natural frequencies.

The simulated natural frequencies at first six modes of the SWCT PV module are found to be 10.02 Hz, 18.168 Hz, 31.755 Hz, 31.941 Hz, 40.081 Hz, and 50.782 Hz [see table 4]. The first six mode shapes for SWCT PV module are shown in figure 7.

Table 4. Simulated natural frequencies of SWCT and busbar PV modules (Hz)

Model	Mode Number					
	1	2	3	4	5	6
SWCT PV module	10.02	18.168	31.755	31.941	40.081	50.782
Busbar PV module	9.3774	10.148	12.492	14.647	16.358	17.581

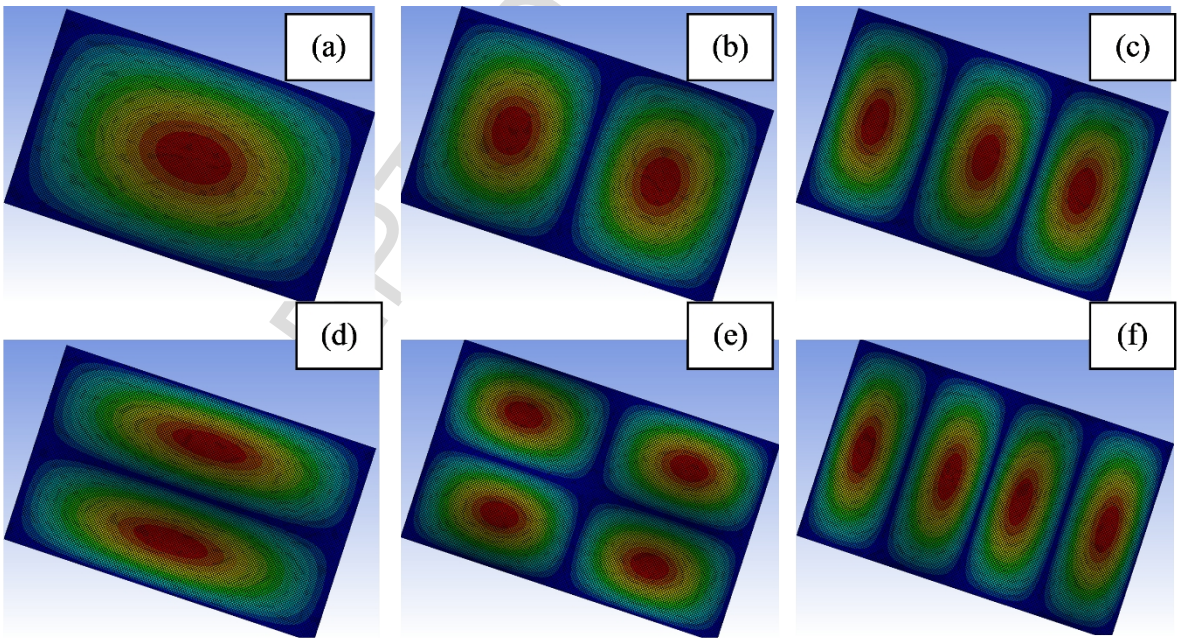

Figure 7. The first six Mode shapes for SWCT PV module (a) first mode (b) second mode (c) third mode (d) fourth mode (e) fifth mode (f) sixth mode.

After modal analysis of SWCT PV module, shocks are simulated as described in section 4.2. During shocks simulation, deflection and stresses occur in different module layers. The maximum displacement in glass is found to be 0.349 mm in the module center, and a minimum of 0.0073 mm is found near the module edges [see figure 8a]. During the time, a maximum displacement of 0.348 mm is found in few solar cells of middle columns and a minimum of 0.0087 mm is found in the cells located at the module edges [see figure 8b]. Furthermore, maximum stresses of magnitude 1.544 MPa and 0.1836 MPa are generated in glass layer and cell matrix respectively [see figure 8c and 8d respectively]. In addition, high stresses (up to 0.756 MPa), and displacements (up to 0.35 mm) are generated in lower wires of middle column cells as compared to other cell wires.

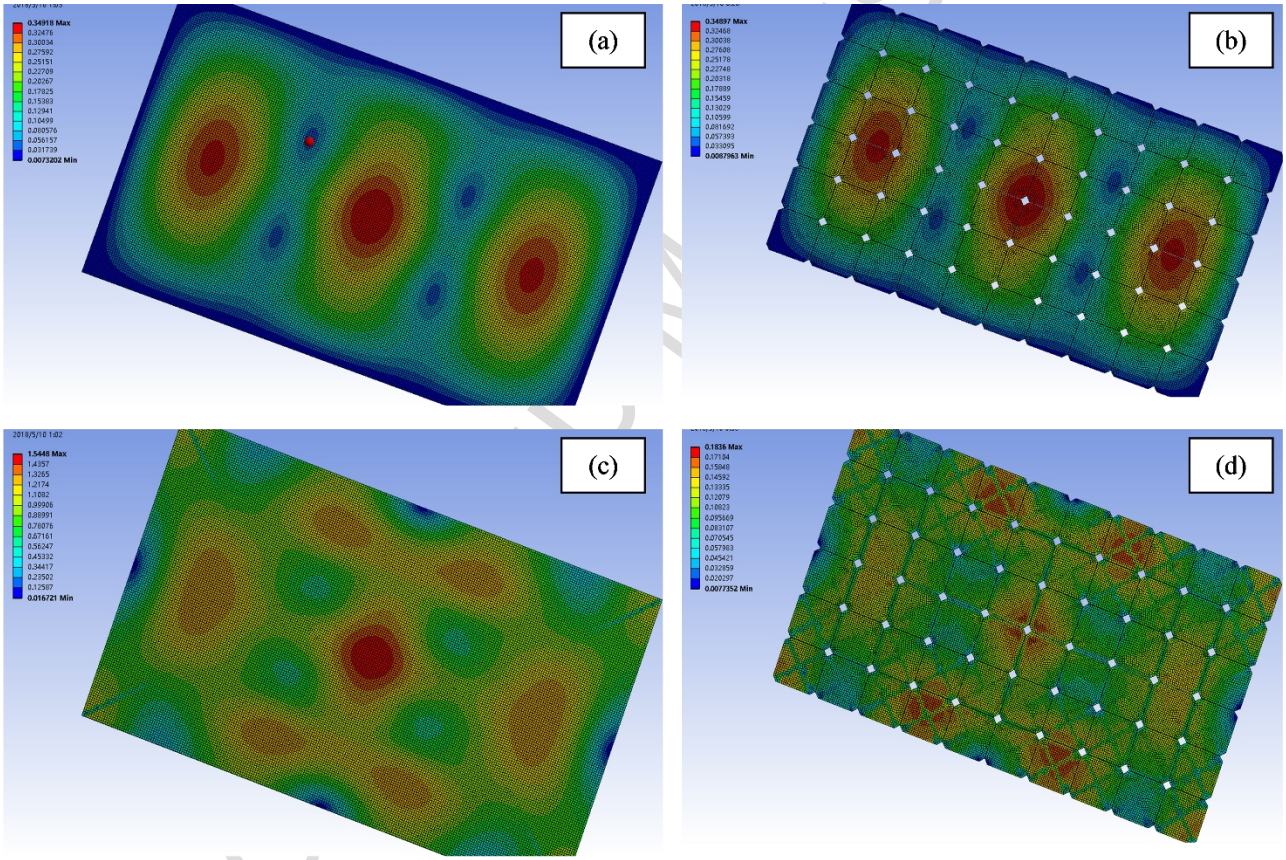

Figure 8. Displacements (mm) and stresses (MPa) in SWCT PV module during transport (a) displacement in glass (b) displacement in solar cells (c) stresses in glass (d) stresses in solar cells.

The simulated natural frequencies at first six modes of the busbar PV module are found to be 9.3774 Hz, 10.148 Hz, 12.492 Hz, 14.647 Hz, 16.358 Hz, and 17.581 Hz [see table 4]. The first six mode shapes for busbar PV module are shown in figure 9.

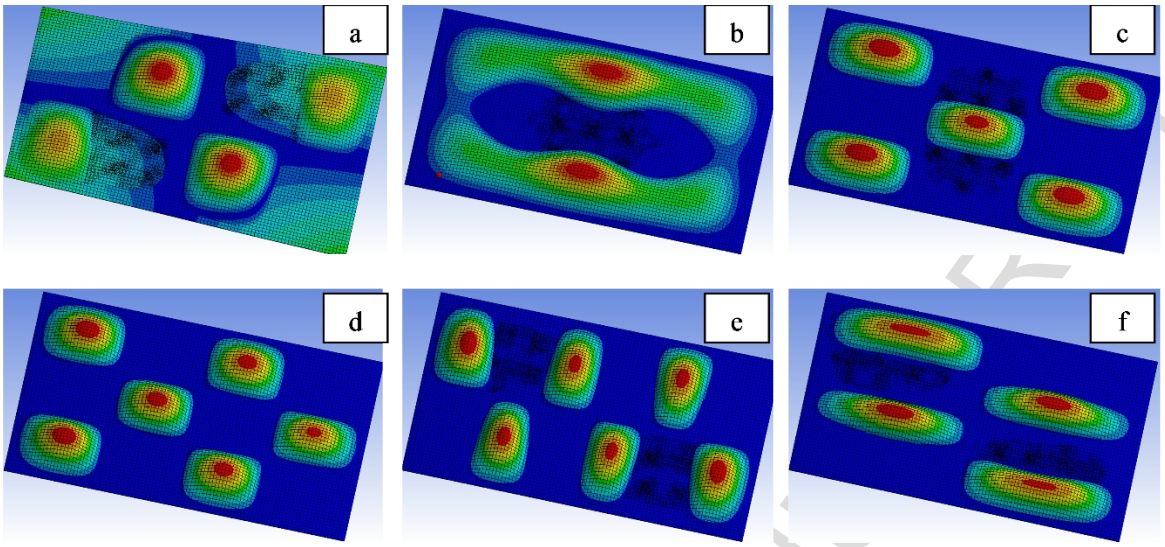

Figure 9. The first six Mode shapes for busbar PV module (a) first mode (b) second mode (c) third mode (d) fourth mode (e) fifth mode (f) sixth mode.

Subsequent to modal analysis of busbar PV module, the maximum amplitude of shocks is varied as described in section 4.2, which causes deflection, and stress generation in different module layers. Maximum stresses of magnitude 0.314 MPa and 2.396 MPa are generated in glass layer and cell matrix respectively [see figure 10a and 10b respectively]. The maximum displacement in glass is found to be 0.21 mm near the module corners and a minimum of 0 mm is found in the center region. During the time, a maximum displacement of 0.52 mm is found in solar cells located at the module corners and a minimum of 0.012 mm is found in the cells located around the module center.

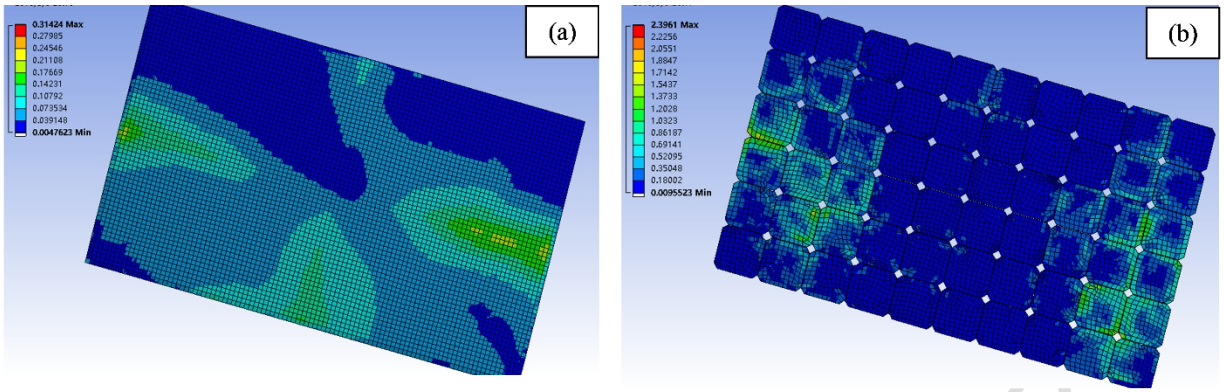

Figure 10. Stresses (MPa) generated in busbar PV modules during transportation (a) stress in glass (b) stress in solar cells.

5.3 Static Loading

The thermo-mechanical performance of the SWCT and busbar PV modules is investigated during IEC 61215 [50] mechanical load test. Figure 11 shows the simulated results of static analysis for SWCT module under a uniform pressure loading in accordance to IEC 61215 [50] standard. In solar cell matrix, higher stresses are found in the solar cells located along the frame [see figure 11a]. A maximum tensile stress of 63.1 MPa is found in these solar cells. However, in other cells, compressive stresses of magnitude 0.01 MPa are found. Moreover, the solar cells located around module center undergo large displacement comparatively. While, the displacement in cells decreases as we move towards module corner leading to least deformation in the cells at module corners.

On the other hand, at glass top, tensile stresses of magnitude up to 12.19 MPa are found near module edges and negligible compressive stresses are found near the module center [see figure 11b]. While, at glass bottom, tensile stresses of magnitude up to 14.18 MPa are found in the center region. However, the glass bottom experiences low stresses near the module edges [see figure 11c]. The tensile strain from the glass bottom is transferred to encapsulant.

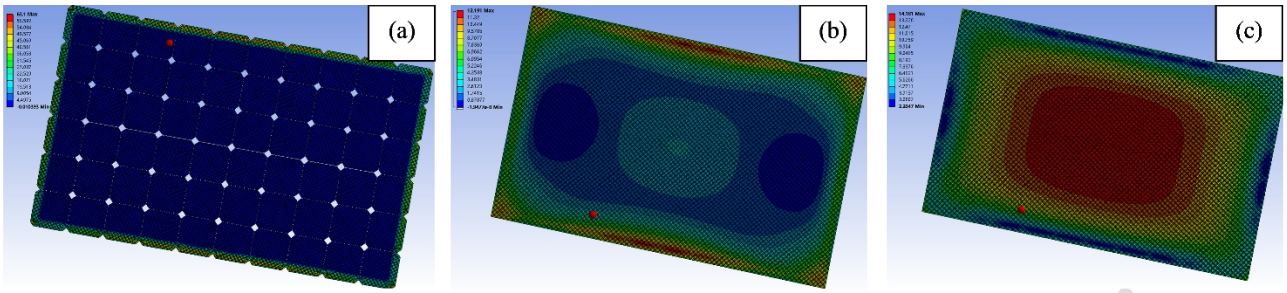

Figure 11. Simulated stresses (MPa) in SWCT PV module during static loading (a) stresses in SWCT solar cells (b) stresses at glass top (c) stresses at glass bottom

Figure 12 shows the results of static analysis for busbar PV module. Higher stresses are found in the solar cells located near the module corners [see figure 12a]. A maximum stress of 68.44 MPa is found in these cells. At glass top side, maximum tensile stresses of magnitude 39.19 MPa are found in the corner regions [see figure 12b], and at glass bottom side, compressive stresses are found in the corner regions and tensile stresses up to 41.6 MPa are found in the center. Moreover, the glass center undergoes high deflection as compared to the glass corners.

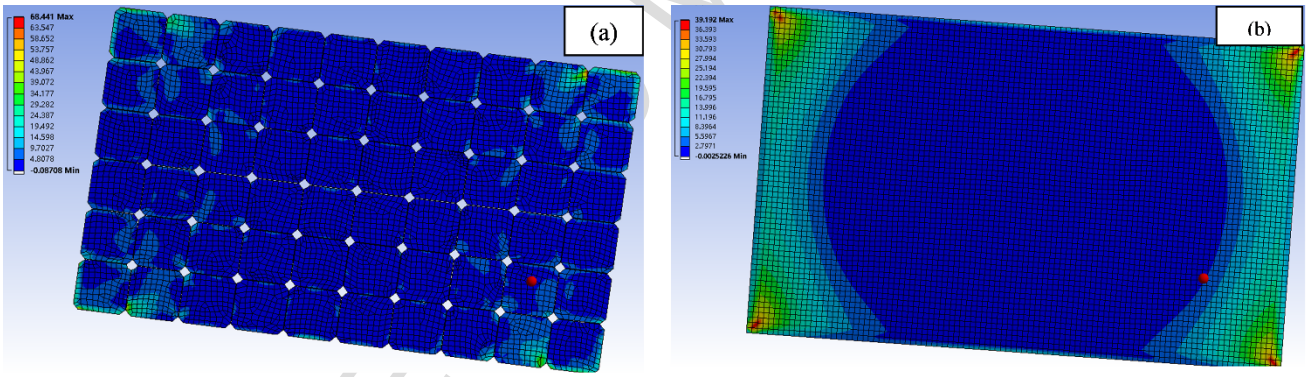

Figure 12. Simulated stresses (MPa) in busbar PV module during static loading (a) stresses in SWCT solar cells (b) stresses at glass top.

5.4 Dynamic loading

Dynamic loads are simulated on both SWCT and busbar PV modules as mentioned in section 4.4. A harmonic excitation with amplitude of 2400 pa and frequency sweep from 0 to 100 Hz is employed to investigate the effects of dynamic loads. During the time, in SWCT PV module, solar cells located in

the corners experience high stresses comparatively. A maximum stress of 50.56 MPa is observed in the corner cells. The stress distribution diagram of solar cell matrix is shown in figure 13a. Moreover, maximum cell displacement of 3.49 mm is observed in the cell matrix [see figure 13b].

In glass, a maximum stress of 54.5 MPa, and a minimum of 0.47 MPa is found. The stress distribution in glass is shown in figure 13c. Furthermore, the glass undergoes maximum displacement of 4.8 mm and a negligible displacement approaching to zero is found near the module edges. The glass displacement due to dynamic loads is shown in figure 13d.

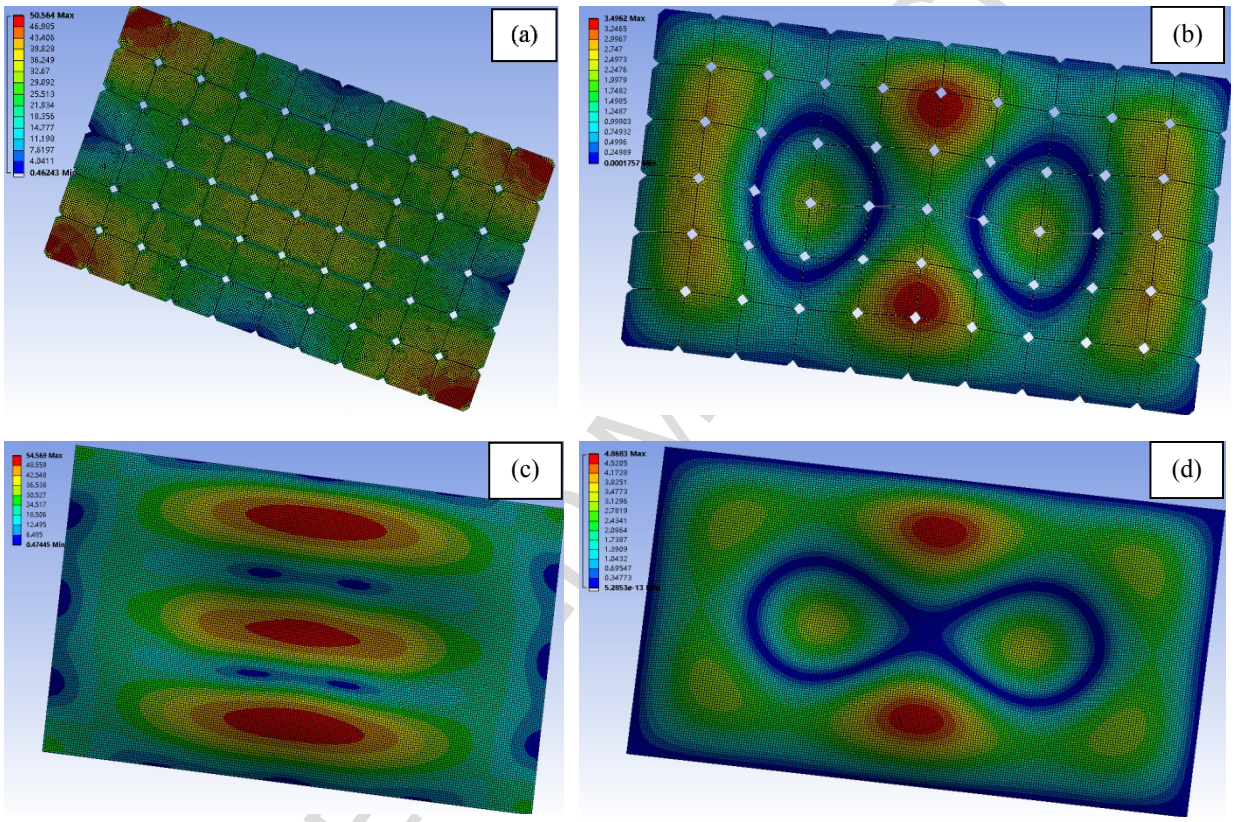

Figure 13. Stresses (MPa) and displacements (mm) in SWCT PV module during dynamic loading (a) Stress in solar cells (b) Displacement in solar cells (c) Stress in glass (d) Displacement in glass

On the other hand, in Busbar PV module, stresses up to 72 MPa are found in solar cells. Therein, higher stresses are found in the cells located near the edges along module width and least stresses are found in the cells of 1st and 6th column [see figure 14a]. Moreover, maximum displacement of 8.15 mm is found in the solar cells [see figure 14b]. During the time, in glass, maximum stresses of magnitude 25.72 MPa are generated near the edges along module width and stresses of magnitude around 12 MPa

are found in center region [see figure 14c]. Moreover, maximum glass displacement of 6.31 mm is found near the edges along module length, and a minimum of 2.7 mm is found in the center [see figure 14d].

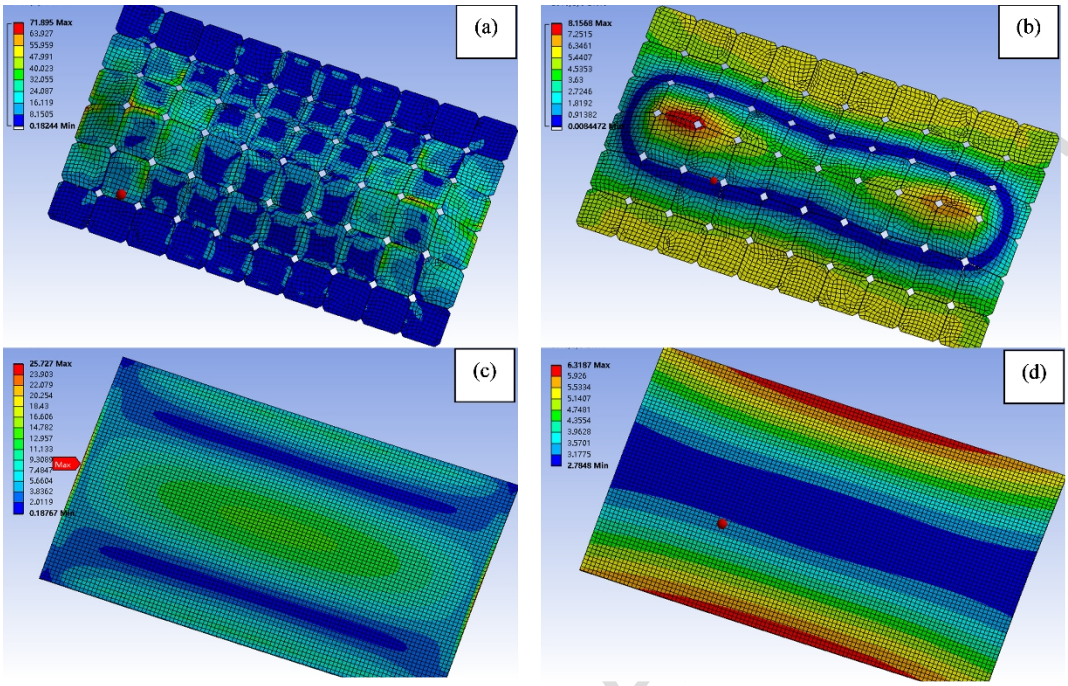

Figure 14. Stresses (MPa) and displacements (mm) in busbar PV module during dynamic loading (a) Stress in solar cells (b) Displacement in solar cells (c) Stress in glass (d) Displacement in glass.

5.5 Thermal Loading

The SWCT and busbar PV modules are subjected to one IEC 61215 [50] temperature cycle. During the time, in SWCT PV module, stresses up to magnitude of 4.5 MPa are generated. In solar cell matrix, stresses up to 1.28 MPa are generated. High stresses are found in the cells located in the middle columns [see figure 15a]. Moreover, the solar cells undergo displacement up to 0.101 mm. Large displacements are found in the cells located at edges along module length and middle columns [see figure 15b]. The encapsulant experiences maximum stresses of 0.27 MPa in the region between cells [see figure 15c] and displacement of 0.07 mm in the center and edges. In addition, the glass undergoes maximum deformation of 0.037 mm in the center and a minimum of 0.02 mm near the edges [see figure 15d]. In copper wires, highest deflection is found in the middle column wires (3rd and 4th col). Therein, maximum deformation is 0.068 mm, near the wire end [see figure 15e]. On the other hand,

comparatively lower deformation values are found in wires located near module edges. Within each cell, higher displacements are observed in the corner wires near their ends as shown in figure 15e, which shows that these wires are more susceptible to thermal damage.

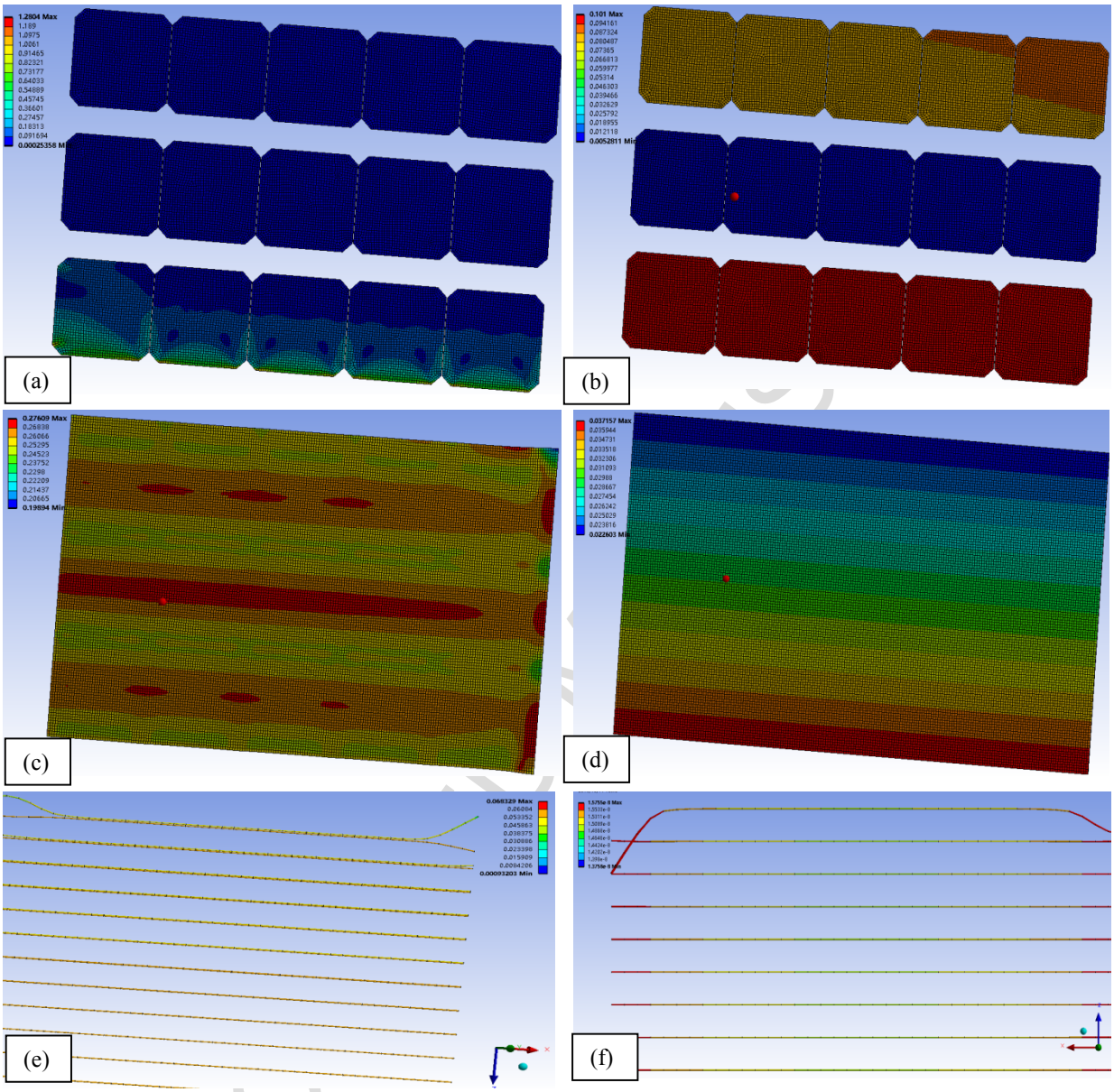

Figure 15. Stresses (MPa), displacements (mm), and strain energy (J) in SWCT PV module after one IEC temperature cycle (a) Stress in solar cells (b) Displacement in solar cells (c) Stress in encapsulant (d) Displacement in glass (e) Deformation in Cu wires (f) Strain energy in Cu wires.

[Upper right-hand quarter of complete module is shown in 15(a, b, c & d)), and Cu wires of a cell located in middle of module are shown in 15(e & f)]

It is reported that thermal cycling has a major effect on interconnection degradation [26, 27]. The thermal loading creates deformation in copper wires and this deformation is stored in the copper wires as strain energy. As the strain energy accumulates upon increased thermal loading, this eventually results in fatigue failure; and larger the strain energy accumulation, the shorter the fatigue life [27]. Strain energy distribution in copper wires of SWCT module after one thermal cycle is shown in figure 15 f. The maximum accumulated strain energy in copper wires after one thermal cycle is $1.57*10^{-8}$ J. The ends of corner wires are more prone to thermal damage as having higher values. For better understanding of strain energy accumulation, plot of maximum strain energy induced in Cu wires of SWCT cell against temperature during first IEC temperature cycle is shown in figure 16. The plot shows that strain energy magnitudes are higher at extreme temperature ends of thermal cycle. Furthermore, it can be observed that for each degree temperature increase/decrease from 25 ^{o}C (standard test condition, STC), there is corresponding rise in maximum strain energy; and after completion of temperature cycle, a strain energy of $1.57 * 10^{-8}$ J is accumulated.

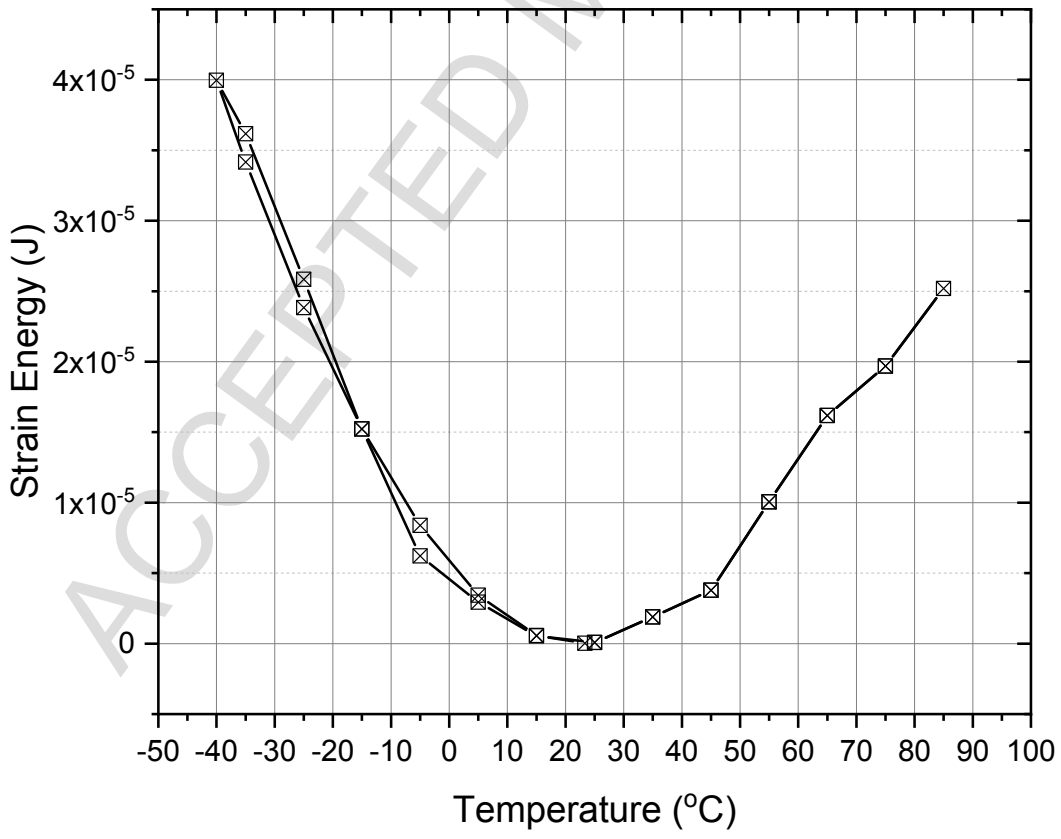

Figure 16. Plot of maximum strain energy (J) in Cu wires of SWCT PV module against temperature during first IEC temperature cycle

In case of busbar PV modules, stresses up to magnitude of 7 MPa are generated in the module after one thermal cycle. Higher stresses are experienced at the edges of module comparatively [see figure 17a]. Stresses up to magnitude of 5.9 MPa are also generated in busbars with maximum values at busbar ends [see figure 17b]. During the time, a cell displacement up to 0.032 mm is also observed in solar cell matrix. The solar cells located at the module edges undergo high deformation comparatively, and the maximum displacement is found in corner cells [see figure 17c]. Furthermore, the glass layer experiences large displacement of magnitude up to 0.2 mm in the central region, and zero displacement at the module edges [see figure 17d]. The solar cells experience maximum stress of 2.72 MPa [see figure 17e].

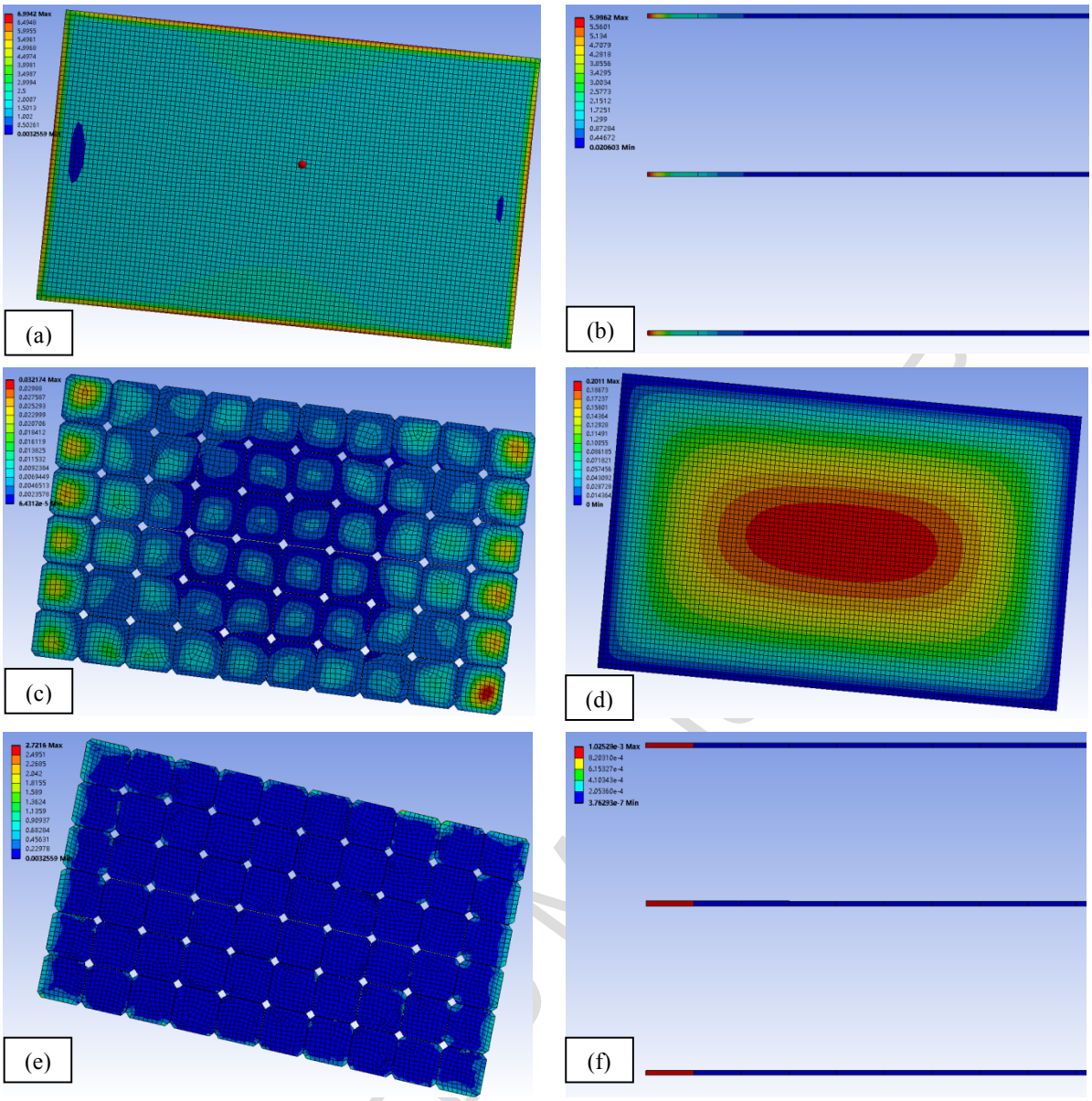

Figure 17. Stresses (MPa), displacements (mm), and strain energy (J) in busbar PV module after one IEC temperature cycle (a) Overall stress in the busbar PV module (b) Stress in the busbars (c) Displacement in the solar cells (d) Displacement in glass (e) Stress in PV cells (f) Strain energy in busbars. [Busbar ends of cells located at corner of module are shown in 16(b & f)]

On the other hand, strain energy distribution in busbars of busbar PV module after one thermal cycle is shown in figure 17 f. The maximum strain energy is $1.025*10^{-3}$ J near busbar ends making this region more susceptible to damage. Plot of maximum strain energy in busbars against temperature during first IEC temperature cycle is shown in figure 18. The graph curve pattern is similar to that of obtained for SWCT copper wire. Strain energy is found higher at extreme ends of cycle. For each degree

temperature increase/decrease from STC, an increase in maximum strain energy is observed; and after cycle completion, a strain energy of $1.025*10^{-3}$ J is accumulated.

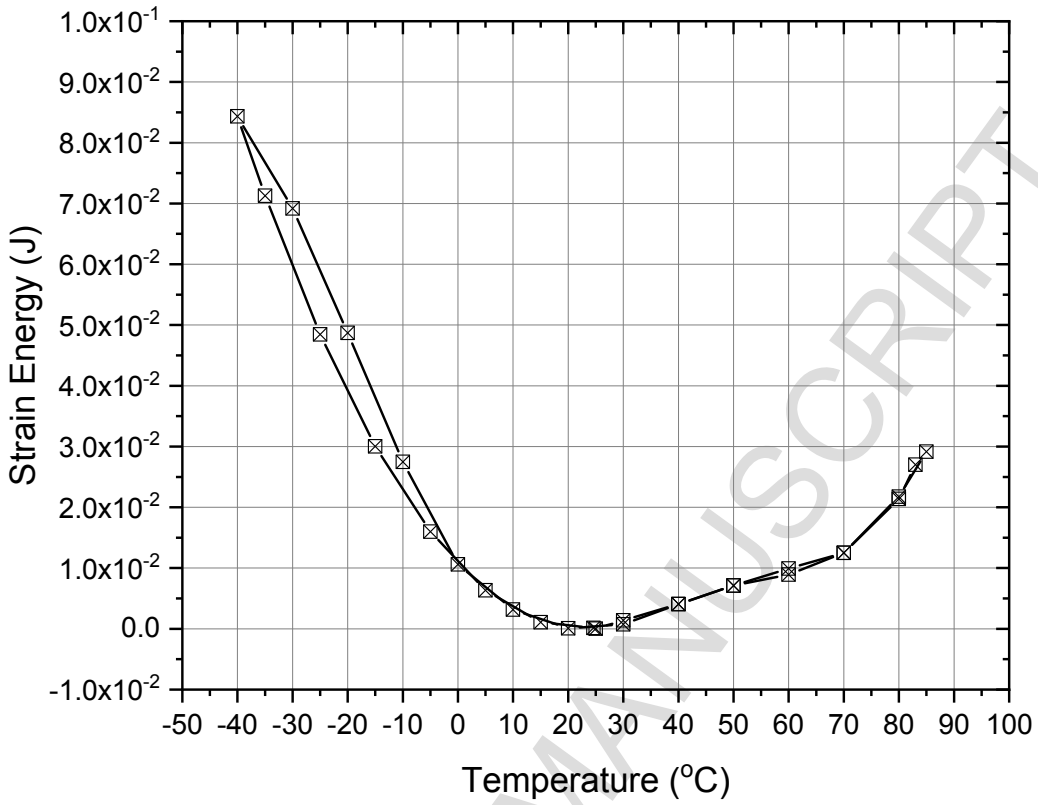

Figure 18. Plot of maximum strain energy (J) in busbars of busbar PV module against temperature during first IEC temperature cycle

5.6 Comparison

This section discusses the comparison between thermo-mechanical behavior of SWCT and busbar modules in response to loads subjected during production, transportation, and subsequent field loads.

Maximum stresses generated in different components of SWCT and busbar PV modules during manufacturing stage are shown in bar graph [see figure 19]. During manufacturing, in SWCT PV module, high stresses are found in solar cells located in the middle columns; and the copper wires over/under the cells located adjacent to frame and in the middle columns experience high stresses. While, during soldering in busbar cells case, high stresses are found at the busbar ends and cell region near the busbar end; and during lamination, the busbar cells located adjacent to module frame

experience higher stresses. The stress accumulation at cell edges is due to bending of interconnectors. These regions seem to be most sensitive to cracks. The cracks developed during production stage due to stress generation may grow later in the field. Thus, process optimization is necessary to prevent cell cracking.

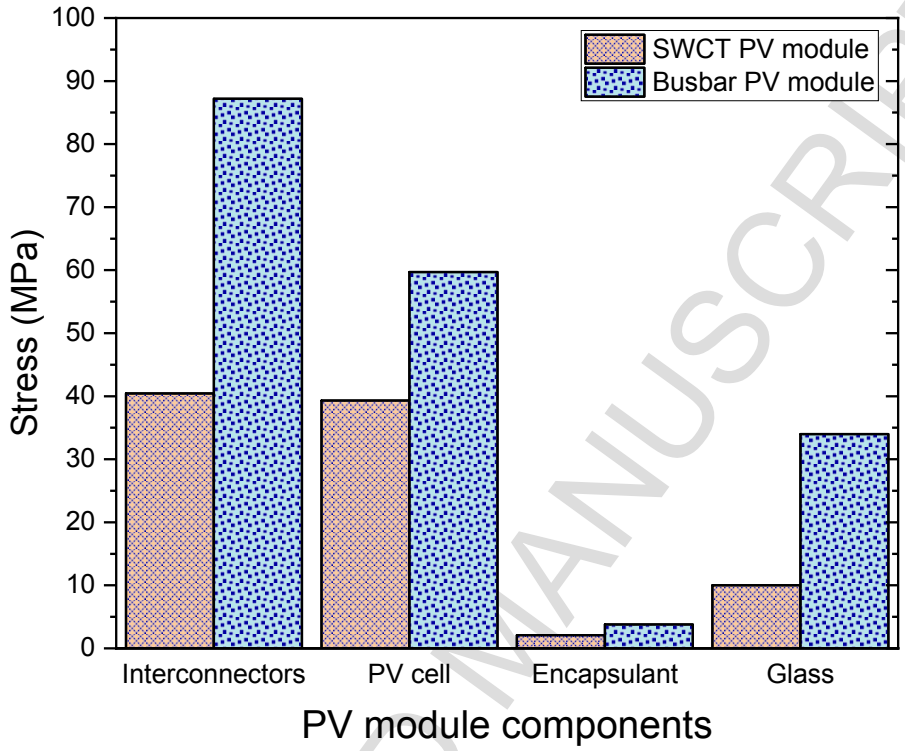

Figure 19. Maximum stresses (MPa) generated in different components of SWCT and busbar PV modules during production stage

Figure 19 shows that the stresses induced in components of SWCT modules are lower which shows that SWCT interconnection technique is relatively a less stress inducing process. The low stress generation in SWCT module during production stage is due to comprisal of low temperature process. The authors [4,5] also state this finding. Thus, its usage can lead to improve the performance and reliability of PV modules which results in longer module life.

During transport stage, in SWCT module, maximum displacements of 0.349 mm and 0.348 mm are found in the glass center and cells located in middle columns respectively. While, in busbar module, maximum displacements of 0.21 mm and 0.52 mm are found in the glass corners and cells located at

module corners respectively. Small cell displacement in SWCT module is due to presence of multiple flexible thin interconnections which improves its reliability as compared to busbars.

Figure 20 presents bar graph comparing maximum stresses generated in SWCT and busbar connected PV cells during module production, static, and dynamic loading stages. It can be clearly seen that relatively less stresses are induced in SWCT connected cells during these stages. During static loading, in SWCT module, maximum stresses are found in the cells located along the frame; while, in busbar module, maximum stresses are found in the solar cells located near the module corners. During dynamic loading, in SWCT module, maximum stresses are found in the cells located at module corners; while, in busbar modules, maximum stresses are found in the cells located near the edges along module width.

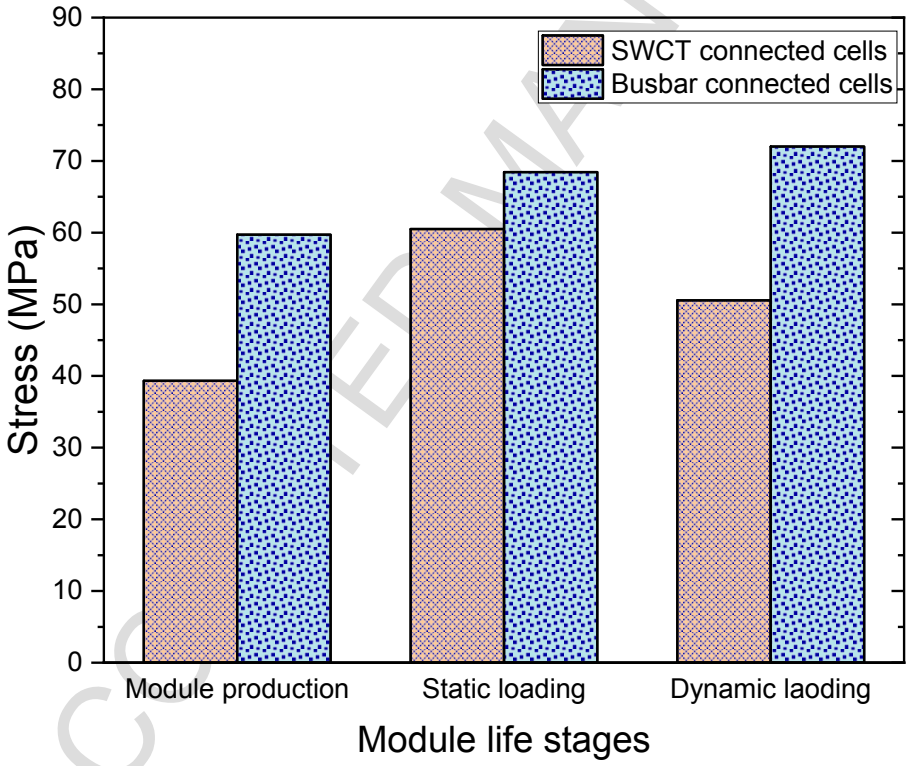

Figure 20. Maximum stresses (MPa) generated in SWCT and busbar connected PV cells during different module life stages.

Figure 21 shows comparison of maximum stresses generated in busbar and SWCT connected PV cells against temperature during first IEC temperature cycle. Higher stress magnitudes are found at extreme

ends of temperature cycle. It shows that temperature deviation from STC affects reliability of PV modules; the greater the temperature deviation from STC, higher the effect on reliability. Moreover, it can be observed from the figure that stress accumulation at the end of thermal cycle is less in SWCT connected cells. Therein, relatively low stress is generated due to large surface contact of round shaped copper wires to encapsulant as compared to rectangular busbars. Walter et al [33] also discussed that the increased surface contact leads to stronger linkage between wires and encapsulant. On the other hand, relatively less strain energy is accumulated in SWCT interconnecting wires making it less prone to thermal damage.

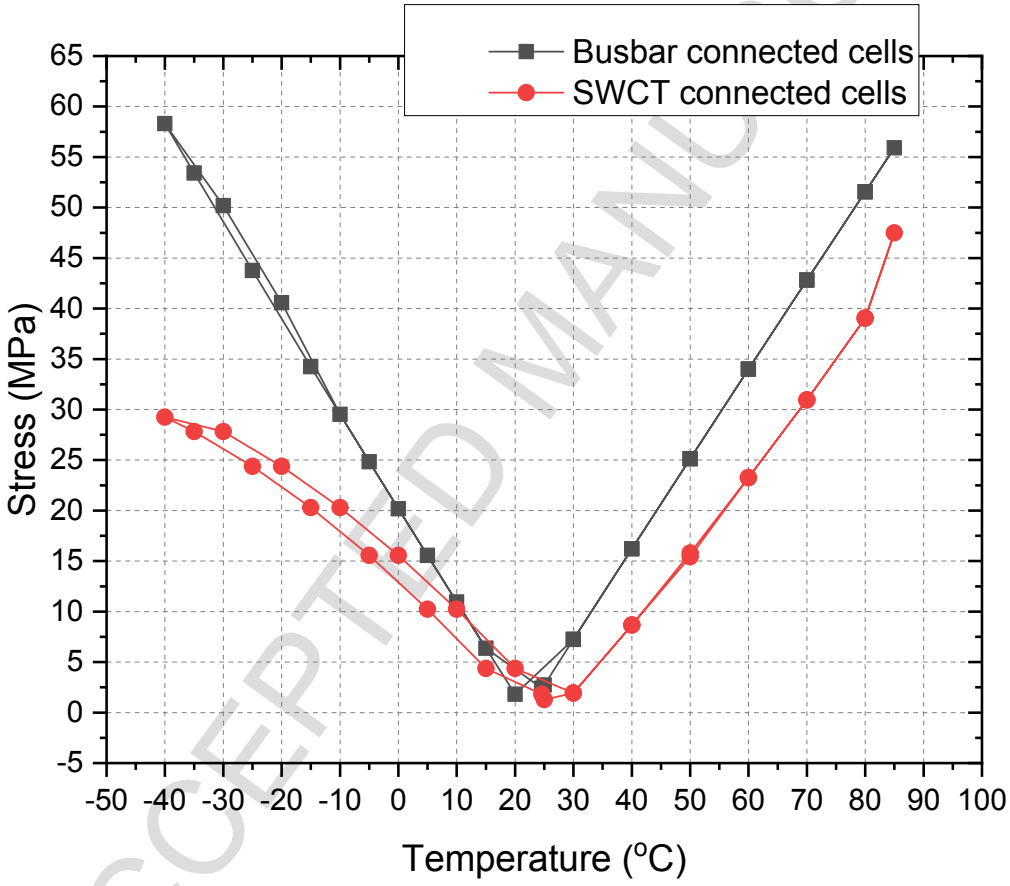

Figure 21. Plot of maximum stresses (MPa) generated in busbar connected PV cells and SWCT connected PV cells against temperature during first IEC temperature cycle.

From comparison, it is found that SWCT interconnection is relatively a less stress inducing process which can lead to improve the performance and reliability of PV modules resulting in longer module life. It has shown potential of generating lower stresses as well as less probability of thermal damage

which enhances the fatigue life of interconnectors. Degradation of solder joints due to thermal loads make cell interconnection reliability a big problem [6], which can be cope up using SWCT interconnection technique. Additionally, it is less prone to dynamic affects due to multiple flexible thin wire arrangement. On the other hand, in case of SWCT modules, silver consumption is reduced by 85 % or more that lowers its production cost [4,5]; and has a minimum shading effect due to round wire geometry, and lower electrical losses leading to efficiency gain [4,5,6]. These all aspects make SWCT a potential alternate of conventional busbar technology.

Conclusion

The present study investigates into thermo-mechanical behavior of SWCT, and busbar PV modules in response to loads subjected during manufacturing, handling, transportation, and subsequent mechanical and thermal loading stages in a consecutive step-by-step manner using finite element modelling approach. Different FE models with consideration of pre-stresses and non-linearities are simulated for these stages. The stresses and displacements experienced by different parts/layers of both modules during these stages are probed. Furthermore, high stressed and crack sensitive regions are identified. Overall, in case of both modules, the solar cells located along module corners and edges, experience high stresses and displacements during lifetime; while, glass experiences high deflection in the center. Following this analysis, the SWCT and busbar modules are compared in terms of response to thermo-mechanical loads during entire module life. The comparison shows that, SWCT module experiences less deformation and stresses throughout entire life due to: comprisal of low temperature production process, presence of multiple flexible thin interconnecting wires, and large surface contact of round shaped Cu wires to encapsulant; indicating advantages of SWCT module in terms of long-term mechanical stability. It has also shown less probability of thermal damage which enhances the fatigue life of interconnectors ensuring cell interconnection reliability. SWCT is found a potential alternate of conventional busbar technology, which can enable enhancement in the reliability and performance of photovoltaic modules for sustainable energy generation.

The results in this work give understanding about thermo-mechanical behavior and stress distribution in SWCT and busbar modules during their entire life; leading to aid the development of enhanced design strategies. The adoption and use of SWCT interconnection technique need to be further studied as a replacement of conventional soldering.

Acknowledgement

The present study was sponsored by the National Natural Science Foundation of China (Grant Nos. 51408578, 51605464, and 51611130195), and Anhui Provincial Natural Science Foundation (1508085QE96). The authors would also like to acknowledge Chinese Academy of Sciences, and the World Academy of Sciences for awarding CAS-TWAS President's fellowship to Ph.D. scholars.

References

[1] Kaule F, Wang W, Schoenfelder S. Modeling and testing the mechanical strength of solar cells. Sol. Energy Mater. Sol. Cells 2014;120:441-447. DOI: 10.1016/j.solmat.2013.06.048.

[2] Schulte-Huxel H, Blankemeyer S, Bock R, Merkle A, Kajari-Schroder S, Brendel R. Aging behaviour of laser welded Al-interconnections in crystalline silicon modules. Sol. Energy Mater. Sol. Cells 2012;106:22–26. DOI: 10.1016/j.solmat.2012.06.021.

[3] Schneider A, Rubin L, Rubin G. Solar cell efficiency improvement by new metallization techniques-The Day4 TM Electrode Concept. Proceedings of the IEEE 4th World Conference on Photovoltaic Energy Conversion. 2006 p.1095-1098. DOI: 10.1109/WCPEC.2006.279333.

[4] Soederstrom T, Papet P, Ufheil J. Smart wire connection technology. Proceedings of the 28th European Photovoltaic Solar Energy Conference and Exhibition (PVSEC). 2013 p.495-499. DOI: 10.4229/28thEUPVSEC2013-1CV.2.17.

[5] Faes A, Despeisse M, Levrat J, Champliaud J, Badel N, Kiaee M, Soderstrom T, Grischke R, Gragert M, Ufheil J, Papet P, Strahm B, Cattaneo G, Cattin J, Baumgartner Y, Yao Y, HesslerWyser A, Ballif C. SmartWire Solar Cell Interconnection Technology. Proceedings of the 29th European

Photovoltaic Solar Energy Conference and Exhibition (PVSEC). 2014 p.2555-2561. DOI: 10.4229/EUPVSEC20142014-5DO.16.3.

[6] Zarmai MT, Ekere NN, Oduoza CF, Amalu EH. A review of interconnection technologies for improved crystalline silicon solar cell photovoltaic module assembly. Applied Energy 2015;154:173-182. DOI: 10.1016/j.apenergy.2015.04.120.

[7] Dhere NG. Toward GW/year production of CIGS within the next decade. Solar Energy Materials and Solar Cells 2007;91:1376-1382. DOI: 10.1016/j.solmat.2007.04.003.

[8] Popovich VA, Yunus A, Janssen M, Richardson IM, Bennett IJ. Effect of silicon solar cell processing parameters and crystallinity on mechanical strength. Solar Energy Materials and Solar Cells 2011;95:97-100. DOI: 10.1016/j.solmat.2010.04.038.

[9] Song WJR, Tippabhotla SK, Tay AAO, Budiman AS. Numerical Simulation of the Evolution of Stress in Solar Cells During the Entire Manufacturing Cycle of a Conventional Silicon Wafer Based Photovoltaic Laminate. IEEE Journal of Photovoltaics 2018;8:210-217. DOI: 10.1109/JPHOTOV.2017.2775158.

[10] Esfahani SN, Asghari S, Rashid-Nadimi S. A numerical model for soldering process in silicon solar cells. Solar Energy 2017;148:49-56. DOI: 10.1016/j.solener.2017.03.065.

[11] Tippabhotla SK, Radchenko I, Song WJR, Illya G et al. From cells to laminate: probing and modeling residual stress evolution in thin silicon photovoltaic modules using synchrotron X-ray micro-diffraction experiments and finite element simulations. Progress in Photovoltaics: research and applications 2017;25:791-809. DOI: 10.1002/pip.2891.

[12] Beinert AJ, Romer P, Buchler A, Haueisen V, Aktaa J, Eitner U. Thermomechanical stress analysis of PV module production by Raman spectroscopy and FEM simulation. Energy Procedia 2017;124:464-469. DOI: 10.1016/j.egypro.2017.09.282.

[13] Lee Y, Tay Andrew AO. Stress Analysis of Silicon Wafer-Based Photovoltaic Modules Under IEC 61215 Mechanical Load Test. Energy Procedia 2013;33:265-271. DOI: 10.1016/j.egypro.2013.05.067.

[14] Rendler LC, Kraft A, Ebert C, Wiese S, Eitner U. Investigation of thermomechanical stress in solar cells with multi busbar interconnection by finite element modeling. Proceedings of the 32nd European Photovoltaic Solar Energy Conference and Exhibition (PVSEC). 2016 p.94-98. DOI: 10.4229/EUPVSEC20162016-1CO.11.2.

[15] Rendler LC, Walter J, Geipel T, Volk M, Ebert C, Eitner U. Modelling and verification of mechanical stress induced by soldering of wires for multi busbar interconnection. Proceedings of the 31st European Photovoltaic Solar Energy Conference and Exhibition (EU PVSEC). 2015 p.84-88. DOI: 10.4229/EUPVSEC20152015-1CO.11.2.

[16] Dietrich S, Pander M, Sander M, Zeller U, Ebert M. Stress analysis of encapsulated solar cells by means of superposition of thermal and mechanical stresses. Proceedings of the SPIE Reliability of Photovoltaic Cells, Modules, Components, and Systems VI 2013; vol. 8825: paper 882505. DOI: 10.1117/12.2024319.

[17] Kontges M, Kajari-Schroder S, Kunze I, Jahn U. Crack statistic of crystalline silicon photovoltaic modules. Proceedings of the 26th European Photovoltaic Solar Energy Conference and Exhibition (EU PVSEC). 2011 p.3290-3294. DOI: 10.4229/26thEUPVSEC2011-4EO.3.6.

[18] Molken JI Van, Yusufoglu UA, Safiei A, Windgassen H, Khandelwal R, Pletzer TM, Kurz H. Impact of micro-cracks on the degradation of solar cell performance based on two-diode model parameters. Energy Procedia 2012;27:167-172. DOI: 10.1016/j.egypro.2012.07.046.

[19] Demant M, Oswald M, Welschehold T, Nold S, Bartsch S, Schoenfelder S, Rein S. Micro-cracks in silicon wafers and solar cells: detection and rating of mechanical strength and electrical quality. Proceedings of the 29th European PV Solar Energy Conference and Exhibition (EU PVSEC). 2014 p.390 – 396. DOI: 10.4229/EUPVSEC20142014-2BO.1.3.

[20] Demant M, Welschehold T, Kluska S, Rein S. Microcracks in Silicon Wafers II: Implications on Solar Cell Characteristics, Statistics and Physical Origin. IEEE Journal of Photovoltaics 2016;6:136-144. DOI: 10.1109/JPHOTOV.2015.2465172.

[21] Kajari-schroder S, Kunze I, Eitner U, Kontges M. Spatial and orientational distribution of cracks in crystalline photovoltaic modules generated by mechanical load tests. Solar Energy Materials and Solar Cells 2011;95:3054-3059. DOI: 10.1016/j.solmat.2011.06.032.

[22] Sander M, Dietrich S, Pander M, Ebert M, Bagdahn J. Systematic investigation of cracks in encapsulated solar cells after mechanical loading. Solar Energy Materials and Solar Cells 2013;111: 82-89. DOI: 10.1016/j.solmat.2012.12.031.

[23] Gabor AM, Janoch R, Anselmo A, Lincoln JL et al. Mechanical Load Testing of Solar Panels-Beyond Certification Testing. Proceedings of the IEEE 43rd Photovoltaic Specialists Conference (PVSC). 2016 p.3574-3579. DOI: 10.1109/PVSC.2016.7750338.

[24] Pingel S, Zemen Y, Frank O, Geipel T, Berghold J. Mechanical Stability of Solar Cells within Solar Panels. Proceedings of the 24th European Photovoltaic Solar Energy Conference. 2009 p.3459-3463. DOI: 10.4229/24thEUPVSEC2009-4AV.3.49.

[25] Wohlgemuth JH, Cunningham DW, Placer NV, Kelly GJ, Nguyen AM. The effect of cell thickness on module reliability. Proceedings of the 33rd IEEE Photovoltaic Specialists Conference. 2008 p.1-4. DOI: 10.1109/PVSC.2008.4922770.

[26] Ogbomo OO, Amalu EH, Ekere NN, Olagbegi PO. Effect of operating temperature on degradation of solder joints in crystalline silicon photovoltaic modules for improved reliability in hot climates. Solar Energy 2018;170:682-693. DOI: 10.1016/j.solener.2018.06.007.

[27] Zarmai MT, Ekere NN, Oduoza CF, Amalu EH. Evaluation of thermo-mechanical damage and fatigue life of solar cell solder interconnections. Robot Comput Integr Manuf 2017;47:37-43. DOI: 10.1016/j.rcim.2016.12.008.

[28] Amalu EH, Hughes DJ, Nabhani F, Winter J. Thermo-mechanical deformation degradation of crystalline silicon photovoltaic (c-Si PV) module in operation. Engineering Failure Analysis 2018;84:229-246. DOI: 10.1016/j.engfailanal.2017.11.009.

[29] Walter J, Tranitz M, Volk M, Ebert C, Eitner U. Multi-wire Interconnection of Busbar-free Solar Cells. Energy Procedia 2014;55:380-388. DOI: 10.1016/j.egypro.2014.08.109.

[30] Rendler LC, Kraft A, Ebert C, Eitner U, Wiese S. Mechanical stress in solar cells with multi busbar interconnection-Parameter study by FEM simulation. Proceedings of the 17th International Conference on Thermal, Mechanical and Multi-Physics Simulation and Experiments in Microelectronics and Microsystems. 2016 p.1-5. DOI: 10.1109/EuroSimE.2016.7463325.

[31] Cattaneo G, Faes A, Heng-Yu L, Galliano F, Gragert M, Yao Y et al. Lamination process and encapsulation materials for glass-glass PV module design. Photovoltaics International 2015;27:1-8.

[32] Papet P, Andreetta L, Lachenal D, Wahli G, Meixenberger J, Legradic B et al. New cell metallization patterns for heterojunction solar cells interconnected by the Smart Wire Connection Technology. Energy Procedia 2015;67:203-209. DOI: 10.1016/j.egypro.2015.03.039.

[33] Walter J, Rendler LC, Ebert C, Kraft A, Eitner U. Solder joint stability study of wire-based interconnection compared to ribbon interconnection. Energy Procedia 2017;124:515-525. DOI: 10.1016/j.egypro.2017.09.288.

[34] https://www.ansys.com/academic

[35] Altenbach H, Altenbach J, Kissing W. Mechanics of Composite Structural Element 2nd edition. Singapore: Springer Nature; 2018.
DOI: https://doi.org/10.1007/978-981-10-8935-0

[36] Eitner U. Thermomechanics of photovoltaic modules. University Thesis. Martin Luther University Halle-Wittenberg (der Martin-Luther-Universität Halle-Wittenberg), Germany. 2011. https://d-nb.info/1025202627/34

[37] Lyon KG, Salinger GL, Swenson CA, White GK. Linear thermal expansion measurements on silicon from 6 to 340 K. Journal of Applied Physics 1977;48(3):865-868. https://doi.org/10.1063/1.323747.

[38] Roberts RB. Thermal expansion reference data: silicon 300-850K. Journal of Physics D: Applied Physics 1981;14:163-166.

[39] Okada Y, Tokumaru Y. Precise determination of lattice parameter and thermal expansion coefficient of silicon between 300 and 1500 K. Journal of Applied Physics 1984;56(2):314-320. https://doi.org/10.1063/1.333965.

[40] Schubert A, Walter H, Dudek R, Michel B, Lekc G, Otto J, Mitic G. Thermo-Mechanical Properties and Creep Deformation of Lead-Containing and Lead-Free Solders. Proceedings of the International Symposium on Advanced Packaging Materials (IEEE Cat. No.01TH8562), Braselton, Georgia, USA. 2001 p.129-134. DOI: 10.1109/ISAOM.2001.916562.

[41] Biglari MH, Oddy M, Oud MA, Davis P. Pb-Free Solders Based on SnAgCu SnAgBi SnCu and SnCu for Wave Soldering of Electronic Assemblies. Proceedings of the Electronics Goes Green conference 2000+, Berlin, Germany. 2000 p.73-82.

[42] Eitner U, Kajari-Schroder S, Kontges M, Altenbach H. Thermal Stress and Strain of Solar Cells in Photovoltaic Modules. In: Altenbach H, Eremeyev VA, editors. Shell-like Structures: Non-classical Theories and Applications. Berlin, Heidelberg: Springer; 2011. p.453-468. DOI: 10.1007/978-3-642-21855-2_29.

[43] Perez TO. Mechanical Behavior of Alternative Multicrystalline Silicon Solar Cells. University Thesis. Technische Universitat Bergakademie Freiberg (Freiberg University of Mining and Technology), Saxony, Germany. 2013. http://nbn-resolving.de/urn:nbn:de:bsz:105-qucosa-117455.

[44] Brady GS, Clauser HR, Vaccari JA. Materials Handbook 15th edition. New York, United States: McGraw-Hill Education; 2002.

[45] Wiese S, Kraemer F, Peter E, and Seib J. Mechanical problems of novel back contact solar modules. Proceedings of the IEEE 13th International Conference on Thermal, Mechanical and Multi-Physics Simulation and Experiments in Microelectronics and Microsystems (EuroSimE). 2012 p.1-6. DOI: 10.1109/ESimE.2012.6191770.

[46] Shackelford JF, Alexander W. CRC Materials Science and Engineering Handbook 3rd Edition. Florida, United States: CRC Press; 2000.

[47] Kontges M, Kurtz S, Packard C, Jahn U, Berger KA, Kato K, Friesen T, Liu H, Iseghem MV et al. Review of Failures of Photovoltaic Modules Report IEA-PVPS T13-01:2014. International Energy Agency. (accessed 29 April 2018).

[48] Kontges M, Siebert M, Morlier A, Illing R, Bessing N, Wegert F. Impact of Transportation on Silicon Wafer-Based Photovoltaic Modules. Progress in Photovoltaics: research and applications 2016;24:1085-1095. DOI: 10.1002/pip.2768.

[49] Kontges M, Kunze I, Kajari-Schroder S, Breitenmoser X, Bjorneklett B. The risk of power loss in crystalline silicon based photovoltaic modules due to micro cracks. Solar Energy Materials and Solar Cells 2011;95:1131-1137. DOI: 10.1016/j.solmat.2010.10.034.

[50] IEC 61215. Crystalline silicon terrestrial photovoltaic (PV) modules - design qualification and type approval. International Electrochemical Commission 2005; 2005.

[51] Assmus M, Jack S, Weiss KA, Koehl M. Measurement and simulation of vibrations of PV-modules induced by dynamic mechanical loads. Progress in Photovoltaics: Research and Applications 2011;19:688-694. DOI: 10.1002/pip.1087.

[52] Kilikevicius A, Cereska A, Kilikeviciene K. Analysis of external dynamic loads influence to photovoltaic module structural performance. Engineering Failure Analysis 2016;66:445-454. DOI: 10.1016/j.engfailanal.2016.04.031.

[53] Dong J, Yang H, Lu X, Zhang H, Peng J. Comparative Study on Static and Dynamic Analyses of an Ultra-thin Double-Glazing PV Module Based on FEM. Energy Procedia 2015;75:343-348. DOI: 10.1016/j.egypro.2015.07.382.

Highlights:

- Thermomechanical behavior of SWCT PV modules during their entire life is studied.
- Thermomechanical behavior of busbar PV modules during their entire life is studied.
- Stresses & displacements experienced by different parts are probed.
- Crack sensitive regions are identified.
- Comparison show advantages of SWCT module in terms of reliability and performance.